Contrib Mineral Petrol (2007) 153:369–387
DOI 10.1007/s00410-006-0152-x

ORIGINAL PAPER

Trace-element partitioning between garnet, clinopyroxene and Fe-rich picritic melts at 3 to 7 GPa

J. Tuff · S. A. Gibson

Received: 24 April 2006 / Accepted: 13 October 2006 / Published online: 15 November 2006

Abstract We have determined mineral-melt partition coefficients (*D* values) for 20 trace elements in garnet-pyroxenite run products, generated in 3 to 7 GPa, 1,425–1,750°C experiments on a high-Fe mantle melt (97SB68) from the Paraná-Etendeka continental-flood-basalt (CFB) province. *D* values for both garnet (~$Py_{63}Al_{25}Gr_{12}$) and clinopyroxene (~$Ca_{0.2}Mg_{0.6}Fe_{0.2}Si_2O_6$) show a large variation with temperature but are less dependent on pressure. At 3 GPa, $D^{cpx/liq}$ values for pyroxenes in garnet-pyroxenite run products are generally lower than those reported from Ca-rich pyroxenes generated in melting experiments on eclogites and basalts (~$Ca_{0.3–0.5}Mg_{0.3–0.6}Fe_{0.07–0.2}Si_2O_6$) but higher than those for Ca-poor pyroxenes from peridotites (~$Ca_{0.2}Mg_{0.7}Fe_{0.1}Si_2O_6$). $D^{grt/liq}$ values for light and heavy rare-earth elements are ≤0.07 and >0.8, respectively, and are similar to those for peridotitic garnets that have comparable grossular but higher pyrope contents ($Py_{70–88}Al_{17–20}Gr_{8–14}$). 97SB68 $D^{grt/liq}_{LREE}$ values are higher and $D^{grt/liq}_{HREE}$ values lower than those for eclogitic garnets which generally have higher grossular contents but lower pyrope contents ($Py_{20–70}Al_{10–50}Gr_{10–55}$). *D* values agree with those predicted by lattice strain modelling and suggest that equilibrium was closely approached for all of our experimental runs. Correlations of *D* values with lattice-strain parameters and major-element contents suggest that the wollastonite component and pyrope:grossular ratio exert major controls on 97SB68 clinopyroxene and garnet partitioning, respectively. These are controlled by the prevailing pressure and temperature conditions for a given bulk-composition. The composition of co-existing melt was found to have a relatively minor effect on 97SB68 *D* values. The variations in *D* values displayed by different mantle lithologies are subtle and our study confirms previous investigations which have suggested that the modal proportions of garnet and clinopyroxene are by far the most influential factor in determining incompatible trace-element concentrations in mantle melts. The trace-element partition coefficients we have determined may be used to place high-pressure constraints on garnet-pyroxenite melting models.

Keywords Ferropicrites · Garnet pyroxenite · Partition coefficients · Trace elements

Communicated by Timothy Grove.

J. Tuff · S. A. Gibson
Department of Earth Sciences, University of Cambridge, Downing Street, Cambridge CB2 3EQ, UK

Present Address:
J. Tuff (✉)
Research School of Earth Sciences, The Australian National University, Building 61 Mills Road, Canberra ACT 0200, Australia
e-mail: james.tuff@anu.edu.au

Introduction

The results of experimental and numerical studies of mantle melts and their source regions suggest that, during adiabatic decompression in upwelling mantle plumes and/or at extensional settings, partial melting of peridotite predominantly occurs at depths <120 km (e.g. Takahashi and Scarfe 1985; White and McKenzie 1995; Herzberg and O'Hara 2002). As a consequence of this, and the significant technical difficulties associ-

ated with high-pressure experiments, most investigations of mineral-melt trace-element partitioning have been limited to pressures of ≤3 GPa (e.g. Hart and Dunn 1993; Johnson 1998; Salters and Longhi 1999; Klemme et al. 2002; Pertermann and Hirschmann 2003a). Nevertheless, an increasing amount of experimental and geochemical evidence suggests that the convecting mantle is heterogeneous and that pyroxene- and garnet-rich lithologies may be a significant source region of melts generated at both mid-ocean-ridges and upwelling mantle plumes (Hirschmann and Stolper 1996; Cordery et al. 1997; Campbell 1998; Takahashi et al. 1998; Yaxley 2000; Leitch and Davies 2001). Many pyroxene-rich mantle lithologies have a lower solidus and will therefore melt at higher pressures than anhydrous peridotite (Kornprobst 1980; Hirschmann and Stolper 1996; Hirschmann et al. 2003; Kogiso et al. 2003). Experimental studies have shown that these early-formed Si-rich pyroxenite-derived melts may react with the surrounding peridotite and convert it to an olivine-free pyroxenite (e.g. Yaxley and Green 1998; Yaxley 2000; Kogiso et al. 1998). At high pressures (~5 GPa) the melt contribution from the garnet pyroxenite will dominate that from the surrounding peridotite and produce Fe-rich picritic melts (Gibson et al. 2000).

It has been shown that mineral-melt partition coefficients generally increase with decreasing temperature and increasing melt silica-content (Wood and Blundy 1997; O'Neill and Eggins 2002; Blundy and Wood 2003) but the dependence of these D values on pressure is less significant. In order to model mantle melt generation processes in detail, it is necessary to have a coherent and precise set of mineral-melt trace-element partition coefficients (D values) for appropriate compositions, temperatures and pressures. In pyroxenites and peridotites, clinopyroxene and garnet are the major hosts of REEs, Sr, Y, high-field-strength elements, Hf and Zr.

The contents of Ca and Ti in the garnet structure are believed to affect the partitioning behaviour of highly charged cations (REEs, Zr, Hf, Ti, Nb, Ta, U; van Westrenen et al. 2001; Pertermann et al. 2004). Concentrations of both Ca, Ti and $D^{grt/liq}$ values are high in garnets from eclogites (CaO = 5.6–15.57 wt.% and TiO_2 = 0.49–2.64 wt.%; Pertermann and Hirschmann 2003a, b; Pertermann et al. 2004) and pyroxenites (Ca = 4.87–8.21 wt.% and TiO_2 = 0.1–0.63 wt.%; Hirschmann et al. 2003; Kogiso et al. 2003; Keshav et al. 2004) and are greater than those for peridotites (3.58–5.52 wt.% CaO; ≤0.66 wt.% TiO_2; Takahashi 1986; Walter 1998; Salters and Longhi 1999).

For pyroxenes, contents of Ca, Al and Na are thought to correlate positively with D values for the REEs, Sr, Y, Ti, Th, U, Nb, Zr, Hf and Sc (e.g. Gaetani and Grove 1995; Hill et al. 2000; Pertermann and Hirschmann 2002; Bennett et al. 2004). Clinopyroxenes from 2 to 5 GPa experiments on pyroxenites, eclogites and basaltic rocks in which CaO ≥ 12 wt.%, Al_2O_3 = 7–20 wt.% and Na_2O ≥ ~ 1 wt.% (Hart and Dunn 1993; Hauri et al. 1994; Johnson 1998; Klemme et al. 2002; Pertermann and Hirschmann 2002, 2003a, b; Hirschmann et al. 2003; Kogiso et al. 2003; Pertermann et al. 2004) have similar or higher major element contents to those generated in experiments on peridotites at similar pressures (CaO ≤ 12.7 wt.%, Al_2O_3 = 6.15–9.63 wt.%, Na_2O = 0.3–2.75 wt.%; Takahashi 1986; Walter 1998; Salters and Longhi 1999; Salters et al. 2002).

We have investigated the behaviour of trace-element partitioning in experimental run products of a high-Fe mantle melt (ferropicrite) that is in equilibrium with garnet pyroxenite at pressures between 3 and 7 GPa and at temperatures ranging from 1,425 to 1,750°C (Tuff et al. 2005). The major-element concentrations of garnet and clinopyroxene in the experimental charges were found by Tuff et al. (2005) to vary with pressure and temperature and it is likely that $D^{cpx/liq}$ and $D^{grt/liq}$, at least for trivalent cations (Y, REE, Sr), will be significantly affected by these compositional changes. Importantly, the major-element contents of clinopyroxene and garnet in our run products are intermediate between those present in peridotites and eclogites and allow us to more accurately assess the compositional controls of different mantle lithologies on partition coefficients. The trace-element partition coefficients that we have determined represent original values that are useful in models of pyroxenite melting.

Experimental and analytical procedures

The starting material in our experiments was a ferropicrite (sample 97SB68) from the base of the Early-Cretaceous Paraná-Etendeka CFB succession in NW Namibia (Table 1; Gibson et al. 2000). The sample is petrographically fresh and has a low loss-on-ignition value (0.43 wt.%). It contains euhedral olivine phenocrysts (~30 modal%) that lack disequilibrium or deformation textures and have low forsterite (Fo_{85}) but similar Ni contents (660 ppm) to olivines crystallising from other primary mantle melts (Gibson 2002); assuming a $D^{Ol\text{-}liquid}_{DFe\text{-}Mg}$ of 0.32 (Ulmer 1989) these olivines

Table 1 Compositions (in wt.%) of basalts, picrites, pyroxenites and peridotites used in experimental studies

	1	2	3	4	5	6	7			8	9
	97SB68	KLB-1	KR4003	MIX1G	G2		A	B	C	79–35 g	1,921 KB
SiO_2	46.91	44.48	44.90	45.56	50.05	56.99	56.62	54.77	53.47	46.70	50.00
TiO_2	1.75	0.16	0.16	0.90	1.97	6.30	5.52	5.14	5.02	0.50	2.60
Al_2O_3	9.09	3.59	4.26	15.19	15.76	14.66	15.38	17.12	19.15	18.00	12.60
FeO*[a]	14.90	8.10	8.02	7.77	9.35	7.91	6.20	5.82	5.6 9	8.03	10.80
MnO	0.17	0.12	0.13	0.15	0.17	0.08	0.08	0.07	0.06	0.15	0.24
MgO	14.94	39.22	37.3	16.67	7.90	2.14	4.28	4.31	4.21	9.52	9.39
CaO	8.08	3.44	3.45	11.48	11.74	7.37	7.36	8.84	8.63	12.00	10.90
Na_2O	1.94	0.3	0.22	1.44	3.04	3.99	3.69	3.41	3.32	2.05	2.33
K_2O	0.68	0.03	0.09	0.04	0.03	0.56	0.53	0.46	0.45	0.07	0.48
P_2O_5	0.19	–	–	–	–	–	–	–	–	0.05	–
NiO	0.08	–	–	–	–	–	–	–	–	–	–
Cr_2O_3	–	0.31	0.41	–	–	–	–	–	–	–	–
Total	100.31	99.75	98.94	99.20	100.00	100.00	99.66	99.94	100.00	97.07	99.30
Mg-no.	64	90	89	79	60	33	55	57	57	68	61

[a] FeO* = total Fe as FeO

1 Ferropicrite, Paraná-Etendeka CFB province (Gibson et al. 2000)

2 Fertile spinel lhezolite, Kilborne Hole crater (Takahashi 1986; Hirose and Kushiro 1993; Takahashi et al. 1993)

3 Fertile garnet lhezolite, West Kettle River (Walter 1998)

4 Silica-deficient garnet pyroxenite prepared from natural mineral and rock powders (Kogiso et al. 2003)

5 MORB-like pyroxenite prepared from natural garnet and cpx + natural kyanite and quartz + TiO_2 (Pertermann and Hirschmann 2003a, b)

6 Synthetic mixture similar to a low-degree melt of a quartz eclogite (Pertermann and Hirschmann 2002)

7 Synthetic mixtures based on starting material no. 6 and modified by Pertermann et al. (2004):

A Starting material no. 6 + 10 wt.% pyrope80/grossular20

B Starting material no. 6 + 15 wt.% pyrope50/grossular50

C Composition B + a small amount of Al_2O_3

8 High-alumina basalt, Medicine Lake, California (Hauri et al. 1994)

9 1,921 Kilauea olivine tholeiite (Johnson 1998)

are in equilibrium with the bulk-rock which has Mg/(Mg + Fe) of 65. Clinopyroxenes are found as rare 1 mm, euhedral phenocrysts (< ~5 modal%) of Ti-rich augites (Mg# = 79–61; Gibson et al. 2000). Sample 97SB68 is among the most primitive of the Paraná-Etendeka ferropicrites and an appropriate starting material for studying mantle-melting processes (Tuff et al. 2005).

The ferropicrite melt was found to be in equilibrium with a garnet and clinopyroxene residue at ≥5 GPa (Tuff et al. 2005), so we have studied the trace-element behaviour of 97SB68 at both 5 and 7 GPa. The 3 GPa phase relations of 97SB68 suggest a melt in equilibrium only with clinopyroxene, but runs at this pressure have also been included in our study because (1) the 3 GPa melting behaviour is similar to that at 5 and 7 GPa; (2) the 3 GPa data set is more complete than at higher pressures and allows the trace-element behaviour of clinopyroxene to be examined over a wide temperature range; and (3) we are able to compare our results with previous studies of mineral-melt trace-element partitioning in eclogite (e.g., Klemme et al. 2002; Pertermann and Hirschmann 2002; Pertermann et al. 2004), peridotite (e.g. Salters and Longhi 1999) and basalt (Hart and Dunn 1993; Hauri et al. 1994; Johnson 1998) that have only been undertaken at ≤3 GPa.

Experimental work was conducted using a fO_2-controlled 1 atmosphere furnace, piston-cylinder and multi-anvil apparatus at Tokyo Institute of Technology (Tuff et al. 2005). Piston-cylinder experiments used the ½-inch, talc-Pyrex assembly of Takahashi and Kushiro (1983), with the sample housed in a 1.8 mm O.D. graphite capsule (~4 mm length) and sealed in a Pt container. The pressure medium for multi-anvil experiments was an 18 mm edge-length MgO/Al_2O_3 octahedron with a $LaCrO_3$ heater and ZrO_2 outer sleeve. The sample was again housed in a 1.8 mm O.D. graphite capsule (~2 mm length) and sealed in Pt. 22 runs were undertaken between 3 and 7 GPa and at temperatures ranging from 1,425°C to 1,750°C; seven run products with the largest mineral grains were selected for our trace-element partitioning study (Table 2). Major-element analysis was conducted on polished epoxy-mounted carbon-coated run charges

Table 2 Experimental run conditions

Run no.	Apparatus	Pressure (GPa)	Temperature (°C)	Duration (h)	Run products	Mode
P 529	BE piston	3	1,425[a]	25	cpx	61
					grt	24
					ol	10
					Melt	5
P 511	BE piston	3	1,475	24	cpx	76
					grt	8
					Melt (+qc)	16
P 507	BE piston	3	1,500	24	cpx	30
					Melt (+qc)	70
P 510	BE piston	3	1,525	24	cpx	20
					Melt (+qc)	80
S 1295	SPI 1000	5	1,500	4	cpx	72
					grt	17
					Melt (+qc)	11
S 1300	SPI 1000	5	1,600	4	cpx	55
					grt	18
					Melt (+qc)	27
S 1330	SPI 1000	7	1,750	4	cpx	4
					grt	1
					Melt	95

ol = olivine, *cpx* = clinopyroxene, *grt* = garnet, (*qc*) = quench crystals, *BE piston* = Boyd-England piston cylinder apparatus, *SPI 1000* = SPI 1000 multi-anvil apparatus

[a] Reverse run starting from 1,525°C melt (for 1 h), and cooling to 1,425°C over 12 h, before being held at 1,425°C for 12 h. Modes estimated by mass-balance calculations after Walter (1998)

using a JEOL JXA8800 electron microprobe (EPMA) at Tokyo Institute of Technology (Tuff et al. 2005). Table 3 shows representative major element analyses of phases from the 3 to 7 GPa runs.

Trace-element concentrations in garnet, clinopyroxene and co-existing glass were determined on gold-coated run charges by secondary-ion mass spectrometry (SIMS) using a Cameca IMS-4f ion microprobe at the University of Edinburgh. A primary O^- beam was used with a net impact energy of ~14.5 keV. The energy offset was 75 eV and the energy window was ±20 eV. Primary beam currents were between 2 and 5 nA, resulting in a beam diameter of ~15–20 μm. The following masses were counted: ^{42}Ca, ^{44}Ca, ^{45}Sc, ^{47}Ti, ^{88}Sr, ^{89}Y, ^{90}Zr, ^{93}Nb, ^{138}Ba, ^{139}La, ^{140}Ce, ^{141}Pr, ^{143}Nd, ^{149}Sm, ^{151}Eu, ^{157}Gd, ^{159}Tb, ^{161}Dy, ^{165}Ho, ^{167}Er, ^{171}Yb and ^{175}Lu relative to ^{30}Si, as determined by EPMA (Tuff et al. 2005). Ion yields were calibrated on NIST 610 glass standard. Background counts were monitored using mass 130.5 and were below detectible limits for nearly all determinations. Analyses were carried out on SRM 610 at least three times each day and the relative ion yields were checked against those of standard garnet and clinopyroxene minerals. There was found to be no need for a matrix correction on either the garnets or clinopyroxenes reported here.

Clinopyroxene crystals were large enough (>40 μm) to avoid matrix contamination. In some of the run charges, however, the garnets were only slightly larger than the 15–20 μm beam diameter, a problem encountered in other experimental studies (e.g., Beattie 1994; Klemme et al. 2002). In order to precisely determine crystal locations and reduce the possible contamination of garnet by surrounding phases, high-quality back-scattered electron images were taken before and after analysis (Fig. 1). Matrix contamination was examined using the concentrations of highly incompatible trace elements (e.g. Ba). Crystal analyses that demonstrated matrix contamination were discarded.

Mineral phases in the 3–7 GPa run products appear to be in equilibrium with the surrounding melt. Tuff et al. (2005) calculated Fe–Mg partition coefficients for clinopyroxene and melt ranging from ~0.24 to 0.36, and for garnet and melt from 0.42 to 0.48; these are comparable to those determined in previously published studies (e.g. Takahashi 1986; Herzberg and Zhang 1996; Walter 1998; Kogiso et al. 2003). In addition, phases exhibited systematic trends with pressure and temperature and we found little or no evidence for zoning in the crystals, by examination of either their textures or major-element compositions (Figs. 2, 3), indicating that equilibrium had been reached for most experimental runs (Fig. 1; Tuff et al. 2005).

Results

Trace-element concentrations of minerals and melts in the 97SB68 experimental run products, together with calculated *D* values are shown in Tables 4 and 5, respectively. Only minerals with the least evidence of melt contamination are shown. Errors are shown as one standard deviation and are comparable to those

Table 3 Phase compositions (in wt.%) from all experimental runs

Run no.	Temp. (°C)	n[a]	Phase[b]		SiO_2	TiO_2	Al_2O_3	FeO*	MnO	MgO	CaO	Na_2O	K_2O	NiO	P_2O_5	Cr_2O_3	Total	Mg#[c]	K_d[d]
3 GPa																			
P-510	1,525	5	Melt	80	46.77 (0.92)	2.16 (0.46)	10.06 (0.72)	15.09 (0.74)	0.19 (0.02)	13.98 (0.81)	8.34 (0.93)	1.63 (0.45)	0.45 (0.42)	0.01 (0.01)	0.28 (0.02)	0.10 (0.02)	99.06	62	
	1,525	4	cpx	20	53.15 (0.78)	0.29 (0.03)	5.93 (0.48)	8.22 (0.28)	0.10 (0.04)	21.16 (0.84)	8.64 (0.50)	1.02 (0.06)	0.01 (0.01)	0.01 (0.01)	0.20 (0.02)	0.21 (0.05)	98.95	82	0.36
P-507	1,500	3	Melt	70	39.54 (4.16)	4.06 (1.49)	11.81 (1.51)	20.43 (6.62)	0.17 (0.06)	11.20 (0.85)	8.53 (1.66)	1.93 (0.38)	0.29 (0.29)	0.00 (0.00)	0.17 (0.06)	0.05 (0.02)	98.18	49	
	1,500	5	cpx	30	52.98 (0.50)	0.35 (0.04)	6.30 (0.23)	8.85 (0.17)	0.14 (0.03)	20.15 (0.76)	8.80 (0.48)	1.20 (0.08)	0.02 (0.01)	0.02 (0.02)	0.09 (0.08)	0.19 (0.02)	99.09	80	0.24
P-511	1,475	12	cpx	73	53.26 (0.43)	0.41 (0.04)	6.29 (0.23)	9.27 (0.25)	0.15 (0.05)	19.89 (0.57)	9.20 (0.56)	1.34 (0.07)	0.01 (0.01)	0.01 (0.01)	0.02 (0.01)	0.16 (0.03)	100.01	79	
	1,475	2	grt	8	42.21 (0.09)	0.76 (0.04)	22.86 (0.19)	11.59 (0.39)	0.23 (0.00)	18.25 (0.35)	4.78 (0.17)	0.05 (0.03)	0.00 (0.01)	0.00 (0.00)	0.01 (0.01)	0.35 (0.07)	101.08	74	
P-529	1,525	7	cpx	ND	51.85 (0.12)	0.61 (0.13)	6.53 (0.27)	10.03 (0.22)	0.12 (0.02)	17.70 (0.89)	10.38 (0.69)	1.78 (0.16)	0.01 (0.01)	0.02 (0.03)		0.12 (0.04)	99.14	76	
	–1,425	3	grt	ND	40.64 (0.09)	0.86 (0.20)	22.67 (0.21)	13.14 (0.76)	0.18 (0.01)	17.32 (0.12)	4.87 (0.24)	0.06 (0.02)	0.01 (0.02)	0.01 (0.01)		0.24 (0.09)	100.00	70	
		3	ol	ND	37.49 (0.20)	0.07 (0.01)	0.13 (0.01)	26.02 (0.18)	0.13 (0.00)	36.43 (0.25)	0.28 (0.03)	0.06 (0.02)	0.01 (0.01)	0.01 (0.02)		0.02 (0.04)	100.65	71	
5 GPa																			
S-1300	1,600	6	Melt	30	49.82 (0.20)	1.90 (0.15)	7.99 (0.33)	12.46 (0.46)	0.12 (0.02)	15.88 (0.56)	9.02 (0.70)	1.73 (0.14)	0.14 (0.11)	0.01 (0.02)		0.13 (0.04)	99.20	69	
/S-1314	1,600	12	grt	17	42.18 (0.31)	1.01 (0.19)	22.50 (0.44)	11.80 (0.28)	0.20 (0.05)	17.75 (0.45)	4.77 (0.38)	0.10 (0.03)	0.01 (0.01)	0.02 (0.03)	0.03 (0.01)	0.25 (0.07)	100.61	73	
	1,600	17	cpx	57	54.40 (0.32)	0.45 (0.05)	5.58 (0.28)	8.51 (0.16)	0.11 (0.05)	18.40 (0.27)	10.00 (0.41)	1.91 (0.09)	0.04 (0.01)	0.01 (0.01)	0.02 (0.02)	0.15 (0.03)	99.58	79	
S-1295	1,500	1	Melt	10	51.53	1.22	8.26	11.82	0.18	16.11	8.63	2.04	0.08	0.01	0.11	0.13	100.10	71	
/S-1315	1,500	3	grt	16	42.14 (0.60)	1.15 (0.16)	22.16 (0.16)	12.45 (0.01)	0.24 (0.03)	17.72 (0.08)	4.74 (0.45)	0.16 (0.03)	0.05 (0.04)	0.00 (0.00)	0.11 (0.03)	0.31 (0.18)	101.24	72	0.96
	1,500	8	cpx	69	55.27 (0.20)	0.53 (0.08)	4.70 (0.22)	8.48 (0.41)	0.12 (0.04)	18.22 (0.46)	10.73 (0.51)	1.92 (0.08)	0.03 (0.02)	0.02 (0.02)	0.03 (0.03)	0.15 (0.05)	100.20	79	0.63
7 GPa																			
S-1330	1,750	3	Melt	95	48.43 (1.09)	2.49 (0.69)	7.09 (0.29)	15.97 (1.27)	0.16 (0.10)	14.18 (0.59)	8.83 (0.32)	2.26 (0.15)	0.44 (0.20)	0.02 (0.03)	0.16 (0.07)	0.08 (0.02)	100.12	61	
	1,750	4	grt	1	44.26 (0.32)	0.72 (0.20)	21.55 (0.36)	10.32 (0.15)	0.20 (0.09)	19.02 (0.18)	5.19 (0.13)	0.16 (0.03)	0.01 (0.01)	0.00 (0.01)	0.03 (0.03)	0.29 (0.04)	101.75	77	0.48
	1,750	5	cpx	4	56.39 (0.38)	0.28 (0.05)	5.69 (0.31)	6.81 (0.14)	0.06 (0.04)	17.33 (0.26)	11.40 (0.43)	2.30 (0.07)	0.06 (0.02)	0.02 (0.02)	0.03 (0.03)	0.15 (0.02)	100.52	82	0.35

Numbers in parentheses are one standard deviation

ND Not determined

[a] Number of analyses

[b] Number refers to the modal proportion of the phase, determined by mass balance calculations and X-ray mapped phase analysis

[c] $Mg\# = 100 \times [Mg/(Mg + Fe^{2+})]$

[d] $K_d = (Fe/Mg)_{mineral}/(Fe/Mg)_{melt}$

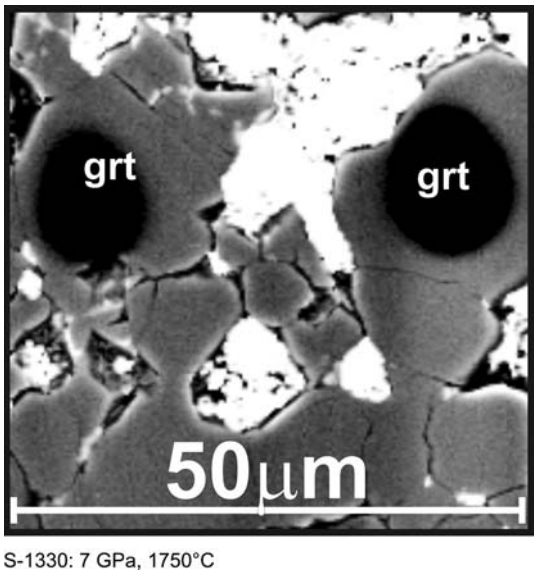

Fig. 1 Back-scattered electron image of run S-1330 (7 GPa, 1,750°C), showing the size of the ion-probe spot (*black circles*) in relation to individual garnet grains

published in previous studies of natural and synthetic starting materials (e.g. Garrido et al. 2000; Hill et al. 2000; Pertermann and Hirschmann 2002). The low variation in trace-element compositions within individual phases suggests that most phase compositions were relatively homogenous and had closely approached equilibrium.

Clinopyroxene and garnet trace-element concentrations and partitioning

Clinopyroxene is the principal mineral host of the light-rare-earth elements (LREEs) and Sr in the experimental charges of 97SB68. Concentrations of Ti are ≤3,029 ppm, Sr < 125 ppm, Zr = 5–30 ppm, La = 0.6–2 ppm and Lu < 0.1 ppm (Table 4). On chondrite-normalised REE plots, the clinopyroxenes are slightly depleted in LREEs and heavy-rare-earth elements (HREEs) relative to middle-rare-earth elements (MREEs; e.g. $[La/Sm]_n$ = 0.48–0.84; $[Sm/Yb]_n$ = 1.67–3.04; Fig. 4)

As expected, the large-ion-lithophile elements and LREEs are strongly incompatible (e.g. $D_{Ba}^{cpx/liq} \leq 0.005$; $D_{La}^{cpx/liq} \leq 0.07$) and the HREEs are moderately incompatible (e.g. $D_{Lu}^{cpx/liq}$ = 0.18–0.38; Table 5). Sc is only compatible at 3 GPa and 1,425°C ($D_{Sc}^{cpx/liq}$ = 1.2). At higher temperatures and pressures it becomes incompatible and $D_{Sc}^{cpx/liq}$ = 0.9–0.6 (Table 5).

Garnets in the 3 to 7 GPa ferropicrite run products are the major hosts of the HREEs (e.g., Lu = 0.4–1 ppm), Sc (50–90 ppm), Y (20–48 ppm) and Zr (50–95 ppm). They also have low contents of Sr (<15 ppm)

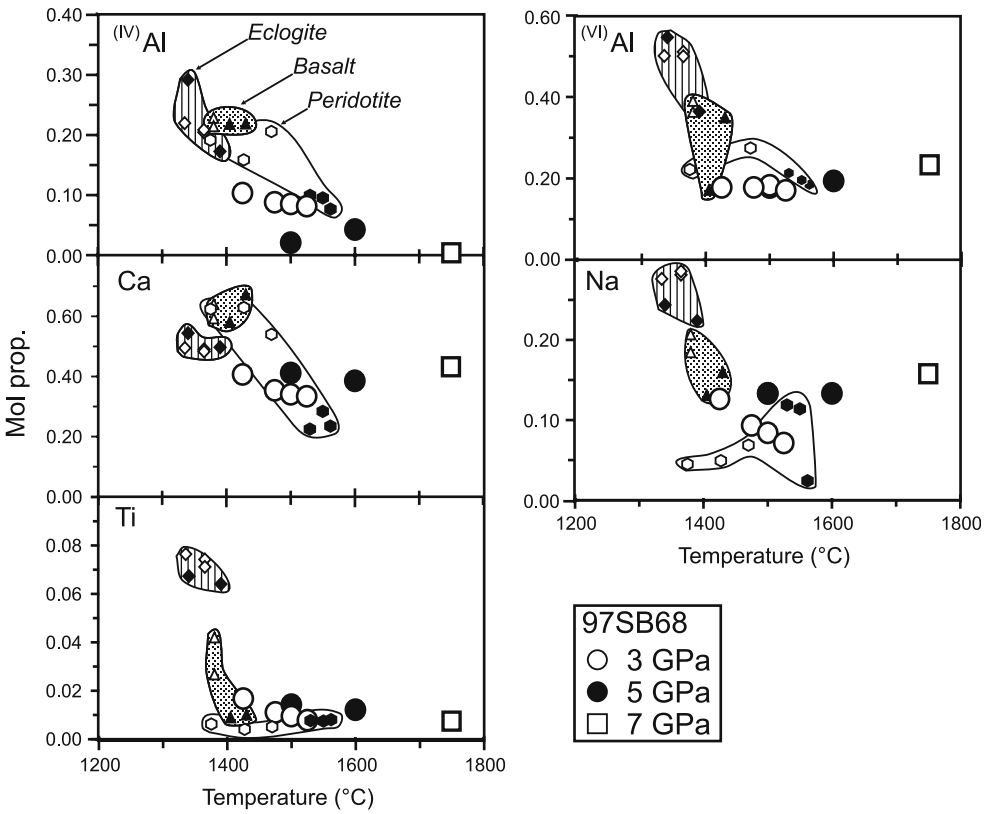

Fig. 2 Variation in major-element content with temperature in clinopyroxenes from 3 to 7 GPa experiments on 97SB68. Also shown are data for: peridotite clinopyroxenes at <2 (*open hexagons*) and 2.8 GPa (*closed hexagons*, Salters and Longhi 1999); quartz eclogite clinopyroxenes at 3 GPa (*open diamonds*, Pertermann and Hirschmann 2002; *closed diamonds*, Pertermann et al. 2004); pyroxenes in alkali basalt at 1.7–2.5 GPa (*open triangles*, Hart and Dunn 1993) and in high-Al basalt at 3 GPa (*closed triangles*, Hauri et al. 1994)

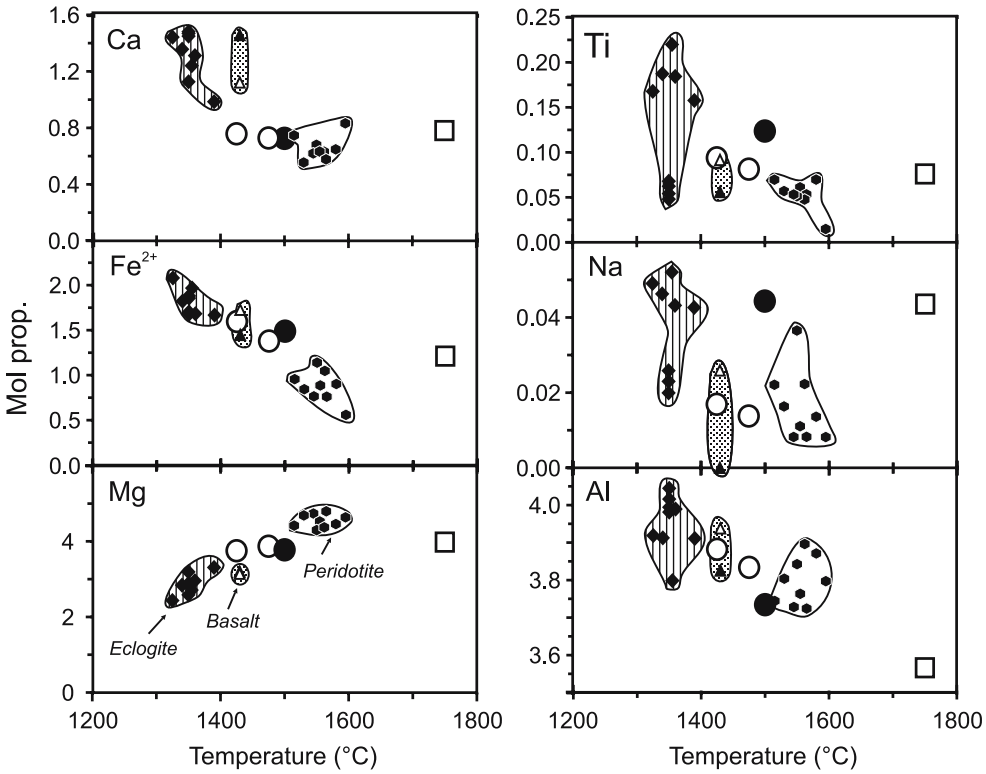

Fig. 3 Variation in major elements with temperature in 97SB68 garnets at 3–7 GPa. Also shown are garnets from experimental runs on peridotite at 2.8 GPa (*closed hexagons*, Salters and Longhi 1999), quartz eclogite at 3 GPa (*closed diamonds*, Pertermann et al. 2004) and basalt at 2.5–3 GPa (*closed triangles*, Hauri et al. 1994; *open triangles*, Johnson 1998)

and LREEs (e.g., La ≤ 0.3 ppm; Table 4). On chondrite-normalised REE plots the garnets are depleted in LREEs relative to MREEs and are slightly depleted in MREEs relative to HREEs (e.g. $[La/Sm]_n$ = 0.06–0.12; $[Sm/Yb]_n$ = 0.34–0.70; Fig. 4). The garnets show a strong compatibility for Sc, Y and the HREEs (e.g. $D_{Lu}^{grt/liq}$ = 1.5–4), moderate incompatibility for the MREEs (e.g. $D_{Sm}^{grt/liq}$ = 0.12–0.24) and strong incompatibility for the LREEs (e.g. $D_{La}^{grt/liq} \leq 0.007$) such that LREE/HREE fractionation is large (Table 5).

Modelling controls on trace-element partitioning: lattice strain model

We have compared the D values determined from the results of our analytical study with those predicted by the lattice strain model of Blundy and Wood (1994) and Wood and Blundy (1997). This model is based on simplified activity-composition relations for the hypothetical pyroxene REEMgSiAlO_6 and has the advantage of eliminating the effect of liquid composition on mineral-melt partitioning (Blundy and Wood 2003). According to Wood and Blundy (1997), the partitioning of an ion with radius r_i into a crystal site is related to the radius of the site (r_o), its apparent Young's Modulus (E) and the strain-free partition coefficient (D_o). For an element with a radius r_i:

$$D_i = D_o \exp\left[\frac{-4\pi E N_A\left[\frac{r_o}{2}(r_i - r_o)^2 + \frac{1}{3}(r_i - r_o)^3\right]}{RT}\right]$$

where N_A is Avogadro's number, R is the universal gas constant and T is the temperature in Kelvin. A non-weighted Levenberg-Marquardt-type, non-linear least-squares fitting routine was employed to derive best-fit values for r_o, D_o and E for the partitioning of trivalent REE and Y. The elements are all assumed to partition into the clinopyroxene M2 site and the garnet X site (Klemme et al. 2002). For clinopyroxenes, r_o varies primarily with crystal composition. Initial r_o values were calculated using Equation 15 of Wood and Blundy (1997):

$$r_o = 0.974 + 0.067X_{M2}^{Ca} - 0.051X_{M2}^{Al}$$

$r_o$in garnet varies with the pyrope-grossular ratio (van Westrenen et al. 1999), but in our 3–7 GPa run products pyrope-grossular ratios vary only slightly (from 84:16 to 86:14; Tuff et al. 2005) and so we have used initial r_o values of between 0.93 and 0.935 in accordance with those of Klemme et al. (2002) and van Westrenen et al. (1999).

The best-fit values for r_o, D_o and E for 3^+ cations for both clinopyroxenes and garnets in 97SB68 run products are shown in Table 6. The values of E for 3 GPa

Table 4 Representative trace-element concentrations (in ppm) of phases

Run no.	P-529			P-511			P-507		P-510	
Pressure (GPa)	3			3			3		3	
Temp. (°C)	1,425			1,475			1,500		1,525	
Phase	cpx	grt	Melt	cpx	grt	Melt	cpx	Melt	cpx	Melt
n[a]	6	4	3	5	3	2	4	4	4	4
Sc	20.93(0.99)	75.16(3.77)	17.54(0.35)	20.30(1.02)	88.96(4.52)	22.69(0.32)	19.70(0.18)	28.79(2.10)	19.51(0.58)	31.75(1.23)
Ti	3,029(92)	4,066(43)	27,285(330)	2,184(72)	4,075(122)	14,647(248)	1,820(38)	15,827(986)	1,834(53)	12,763(231)
Sr	75.56(2.27)	3.36(0.34)	883.12(80)	42.83(1.36)	4.15(0.42)	671.56(56)	38.39(1.88)	695.20(44)	27.80(1.50)	462.77(6.61)
Y	6.01(0.22)	43.12(1.62)	17.36(0.59)	5.29(0.12)	48.16(1.44)	19.77(0.87)	4.85(0.12)	22.24(1.57)	4.36(0.32)	20.23(0.49)
Zr	17.90(0.54)	94.39(0.66)	374.34(26)	11.09(0.14)	79.57(4.85)	245.58(15)	8.18(0.82)	253.72(16)	6.41(0.30)	181.39(3.99)
Nb	0.21(0.01)	0.28(0.01)	35.52(3.76)	0.08(0.001)	0.17(0.05)	22.94(1.07)	0.13(0.01)	22.44(0.58)	0.14(0.05)	16.62(0.35)
Ba	0.85(0.27)	0.80(0.05)	729.48(77)	1.11(0.11)	2.31(0.23)	390.54(20)	0.12(0.03)	424.22(16)	0.77(0.17)	265.01(18)
La	1.48(0.15)	0.22(0.07)	71.65(9.35)	1.19(0.07)	0.26(0.08)	54.86(3.46)	0.74(0.22)	61.36(3.80)	0.73(0.05)	29.71(0.62)
Ce	4.82(0.81)	1.03(0.10)	109.10(11)	2.62(0.04)	0.92(0.28)	68.77(4.95)	2.11(0.07)	70.50(3.52)	1.79(0.26)	50.79(0.96)
Pr	0.87(0.20)	0.38(0.08)	14.10(0.89)	0.45(0.04)	0.29(0.09)	8.39(0.84)	0.43(0.02)	8.79(0.60)	0.34(0.08)	6.75(0.29)
Nd	6.03(0.28)	3.15(0.23)	63.77(3.00)	3.45(0.31)	2.97(0.52)	40.44(2.26)	2.87(0.20)	40.95(2.34)	2.60(0.17)	31.67(1.01)
Sm	1.93(0.19)	2.27(0.19)	12.22(0.27)	1.24(0.07)	1.93(0.18)	8.21(0.51)	0.81(0.24)	8.50(0.74)	0.89(0.04)	6.84(0.42)
Eu	0.68(0.10)	1.01(0.12)	4.52(0.05)	0.36(0.01)	0.82(0.05)	2.61(0.06)	0.31(0.09)	2.84(0.11)	0.30(0.02)	2.38(0.18)
Gd	2.15(0.13)	4.05(0.34)	11.27(0.56)	1.69(0.03)	3.59(0.20)	8.30(0.42)	1.10(0.11)	8.84(0.61)	0.84(0.20)	6.34(0.15)
Tb	0.34(0.03)	0.89(0.08)	1.40(0.13)	0.24(0.05)	1.07(0.03)	1.10(0.04)	0.25(0.03)	1.17(0.01)	0.14(0.02)	0.95(0.07)
Dy	1.52(0.05)	7.71(0.71)	6.63(0.41)	1.65(0.03)	9.57(0.97)	5.83(0.42)	1.52(0.04)	6.71(0.04)	1.15(0.16)	5.41(0.32)
Ho	0.25(0.02)	1.58(0.14)	0.99(0.08)	0.22(0.04)	1.93(0.27)	1.03(0.09)	0.23(0.05)	1.16(0.08)	0.19(0.02)	0.97(0.04)
Er	0.66(0.08)	5.02(0.27)	2.52(0.03)	0.55(0.05)	5.82(0.59)	2.79(0.05)	0.58(0.07)	2.84(0.26)	0.59(0.10)	2.73(0.13)
Yb	0.43(0.11)	4.91(0.28)	1.25(0.27)	0.44(0.08)	6.15(0.09)	1.96(0.29)	0.52(0.01)	2.09(0.21)	0.51(0.06)	2.05(0.19)
Lu	0.07(0.04)	0.77(0.09)	0.19(0.03)	0.09(0.001)	0.98(0.19)	0.31(0.05)	0.08(0.01)	0.30(0.001)	0.08(0.01)	0.32(0.03)

Run no.	S-1295			S-1314			S-1330		
Pressure (GPa)	5			5			7		
Temp. (°C)	1,500			1,600			1,750		
Phase	cpx	grt	Melt	cpx	grt	Melt	cpx	grt	Melt
n[a]	4	3	4	5	ND	2	4	5	4
Sc	20.21(0.10)	52.78(1.98)	30.31(1.87)	18.10(0.26)		25.94(0.36)	15.50(0.53)	56.27(1.90)	26.09(1.38)
Ti	2,666(65)	3,701(66)	15,029(259)	2,552(53)		20,391(188)	1,433(58)	3,385(142)	15,344(55)
Sr	123.17(4.55)	14.67(0.44)	454.62(35)	117.93(3.54)		924.00(14)	94.97(2.85)	4.16(0.42)	716.59(34)
Y	5.11(0.09)	24.99(0.21)	16.22(0.80)	5.20(0.07)		23.65(0.16)	3.31(0.24)	19.92(0.04)	20.36(0.43)
Zr	13.99(0.42)	75.99(4.50)	309.29(26)	29.71(1.01)		401.03(20)	11.52(0.35)	49.11(1.47)	267.15(13)
Nb	0.19(0.08)	0.37(0.11)	21.10(0.53)	0.23(0.07)		31.50(0.84)	0.11(0.02)	0.33(0.13)	24.87(1.40)
Ba	1.80(0.15)	2.33(0.23)	346.60(4.05)	1.37(0.14)		652.56(28)	0.71(0.21)	0.93(0.28)	564.55(28)
La	1.78(0.57)	0.17(0.05)	25.55(1.28)	1.39(0.14)		50.00(2.5)	0.60(0.18)	0.21(0.06)	30.00(1.50)
Ce	5.25(0.52)	0.75(0.23)	48.07(2.40)	4.98(0.18)		104.59(3.53)	2.45(0.21)	0.93(0.003)	75.41(3.98)
Pr	0.77(0.04)	0.21(0.06)	6.63(0.47)	0.87(0.13)		13.03(0.46)	0.47(0.03)	0.18(0.01)	9.68(0.38)
Nd	4.85(0.35)	2.48(0.25)	33.55(1.98)	4.86(0.06)		58.28(2.06)	3.06(0.01)	1.37(0.14)	44.15(1.17)
Sm	1.33(0.03)	1.71(0.08)	7.30(0.35)	1.52(0.21)		11.84(0.55)	0.68(0.05)	1.13(0.14)	9.43(0.23)
Eu	0.47(0.06)	0.61(0.14)	2.36(0.03)	0.41(0.05)		3.89(0.18)	0.33(0.02)	0.44(0.13)	—
Gd	1.38(0.22)	3.00(0.31)	8.00(0.50)	1.36(0.14)		13.05(0.62)	1.02(0.03)	2.18(0.10)	9.88(0.47)
Tb	0.21(0.04)	0.69(0.05)	1.07(0.06)	0.26(0.04)		1.62(0.11)	0.13(0.04)	0.46(0.01)	0.98(0.19)
Dy	1.38(0.14)	4.96(0.10)	5.32(0.37)	1.41(0.06)		8.09(0.25)	0.94(0.16)	3.79(0.11)	4.59(0.23)
Ho	0.22(0.02)	1.06(0.06)	0.85(0.13)	0.22(0.04)		1.13(0.06)	0.16(0.03)	0.85(0.03)	1.03(0.04)
Er	0.57(0.06)	2.90(0.24)	2.28(0.06)	0.54(0.06)		2.40(0.12)	0.38(0.11)	2.35(0.34)	2.30(0.11)
Yb	0.51(0.13)	2.61(0.46)	1.53(0.05)	0.69(0.001)		1.77(0.13)	0.36(0.01)	2.46(0.25)	1.49(0.07)
Lu	0.07(0.01)	0.45(0.05)	0.19(0.03)	0.03(0.01)		0.25(0.04)	0.05(0.01)	0.41(0.03)	0.27(0.04)

Descriptions of runs are given in Table 2

Uncertainties (in brackets) are one standard deviation

ND Not determined

[a] Total number of spots analysed for each phase

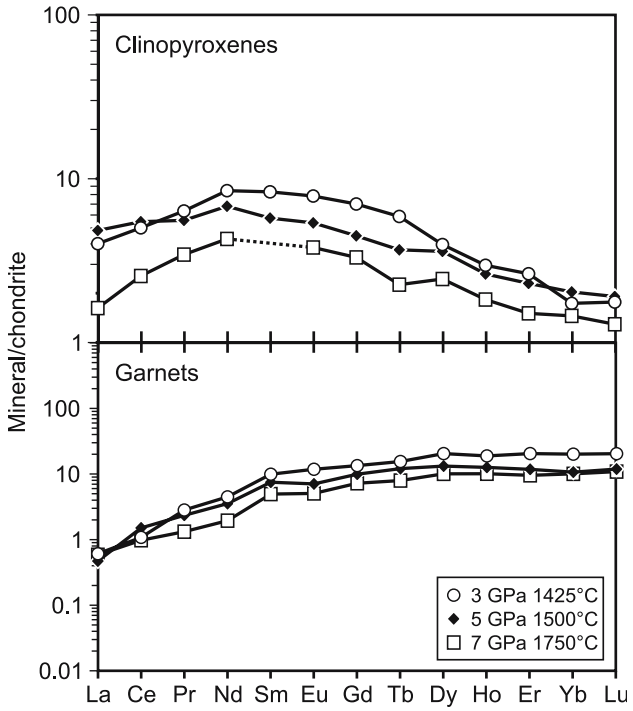

Fig. 4 Chondrite normalised REE plots of 97SB68 clinopyroxenes and garnets at 3, 5 and 7 GPa. Data are from Table 4

clinopyroxenes (~140–320) are similar to those reported for eclogites (Klemme et al. 2002; Pertermann and Hirschmann 2002) and for the Na_2O–CaO–MgO–Al_2O_3–SiO_2 (NCMAS) system (Hill et al. 2000). Overall, 97SB68 clinopyroxene values for D_o (~0.3) and r_o (~0.98) at 3 GPa are lower than those previously reported. Values of r_o generally display a positive correlation with clinopyroxene Ca content and a weak negative correlation with $^{(IV)}$Al content, which correspond to the Wo and CaTs components, respectively (Fig. 5). D_o and E display negative correlations with Ca and Wo, but little or no correlation with $^{(IV)}$Al or CaTs. D_o and r_o display stronger correlations with Wo content than with CaTs, suggesting that the former exerts a greater control. Values of r_o and D_o correlate positively and negatively with temperature, respectively (Fig. 5).

Values of E for 97SB68 garnets at all pressures display a good agreement with those previously reported (e.g. Hill 2000; Klemme et al. 2002; Table 6), although D_o values are lower. Differences in D_o and E may reflect the variations in phase compositions that result from the changes in pressure and temperature of the 97SB68 runs (Wood and Blundy 1997). These variations may also partially reflect the slight change in the pyrope-grossular content of the garnet.

Plots of ionic radius versus $D^{cpx/liq}$ and $D^{grt/liq}$ for REEs, Y and Sc in the experimental run products of 97SB68 are shown in Figs. 6 and 7. Overall, a reasonable agreement is found between the theoretical and experimental values for both mineral phases, indicating that equilibrium was closely approached for most experimental runs (Klemme et al. 2002). Some HREE D values for 97SB68 clinopyroxenes are lower than those predicted by the theoretical values. This may be due to errors in the determination of melt trace-element contents at these pressure and temperature conditions, leading to lower D values. Sc was not used in the non-linear model fitting routines, but has been plotted to test the accuracy of the parabolic curve fits for garnet. Figure 7 shows that Sc fits on the left limb of the model curves at all run conditions.

Discussion

Major-element controls on clinopyroxene D values

Mineral-melt trace element partitioning is strongly linked to the major-element composition of an individual phase, which in turn is controlled by the prevailing pressure and temperature conditions for a given bulk-composition (Klemme et al. 2002; Blundy and Wood 2003). In clinopyroxene, trivalent cations (such as the REEs, Sr and Y) are incorporated in to the M2 site and their partitioning is dependent on the amount of replacement of Si by $^{(IV)}$Al or Ca by Na. Previous studies have noted increased partitioning of these trivalent cations with increases in the wollastonite ($CaSiO_3$; Wo) and Ca-Tschermak ($CaAl_2SiO_6$; CaTs) components (e.g. McKay et al. 1986; Gallahan and Nielsen 1992; Jones and McKay 1992; Lundstrom et al. 1994; Gaetani and Grove 1995; Blundy et al. 1996; Wood and Blundy 1997; Hill et al. 2000). Although Bennett et al. (2004) found no simple correlation between trace-element partition coefficients and the jadeite ($NaAlSi_2O_6$) content in pyroxene, it was noted that partitioning of trivalent, tetravalent and to a lesser extent, divalent cations in pyroxene increases with increasing Na_2O concentrations.

$D^{cpx/liq}$ values for the LREEs (< ~0.1), MREEs (< ~0.3) and Zr (< ~0.05) in 3 GPa run products of 97SB68 are lower than those determined in previous studies of eclogites and basalts, undertaken at comparable temperatures (1,200–1,470°C) and pressures. The overall patterns displayed by D values on multi-element plots are, however, similar (Fig. 8; Hart and

Table 5 Mineral/melt partition coefficients

Run no.	P-529	P-511	P-507	P-510	S-1295	S-1314	S-1330	P-529	P-511	S-1295	S-1330
P (GPa)	3	3	3	3	5	5	7	3	3	5	7
T (°C)	1,425	1,475	1,500	1,525	1,500	1,600	1,750	1,425	1,475	1,500	1,750
Mineral	cpx	cpx	cpx	cpx	cpx	cpx	cpx	grt	grt	grt	grt
Sc	1.193(0.081)	0.895(0.058)	0.684(0.056)	0.614(0.042)	0.667(0.044)	0.698(0.020)	0.594(0.052)	4.285(0.30)	3.921(0.26)	1.741(0.17)	2.157(0.19)
Ti	0.111(0.005)	0.149(0.007)	0.115(0.010)	0.144(0.007)	0.177(0.008)	0.125(0.004)	0.093(0.004)	0.149(0.003)	0.278(0.013)	0.246(0.009)	0.221(0.010)
Sr	0.086(0.010)	0.064(0.007)	0.055(0.006)	0.060(0.004)	0.271(0.031)	0.128(0.006)	0.133(0.013)	0.004(0.0007)	0.006(0.001)	0.032(0.003)	0.006(0.0009)
Y	0.346(0.024)	0.268(0.018)	0.218(0.021)	0.216(0.021)	0.315(0.021)	0.220(0.004)	0.163(0.015)	2.483(0.18)	2.436(0.18)	1.541(0.089)	0.978(0.022)
Zr	0.048(0.010)	0.045(0.003)	0.032(0.005)	0.035(0.002)	0.045(0.005)	0.074(0.006)	0.043(0.003)	0.252(0.019)	0.324(0.040)	0.246(0.035)	0.184(0.014)
Nb	0.006(0.0009)	0.003(0.0002)	0.006(0.0005)	0.009(0.003)	0.009(0.004)	0.007(0.003)	0.005(0.001)	0.008(0.001)	0.007(0.003)	0.017(0.006)	0.013(0.006)
Ba	0.001(0.0005)	0.003(0.0004)	0.0003(0.0001)	0.003(0.0008)	0.005(0.0005)	0.002(0.0003)	0.001(0.0004)	0.001(0.0002)	0.006(0.0009)	0.007(0.0007)	0.002(0.0006)
La	0.021(0.005)	0.022(0.003)	0.012(0.004)	0.024(0.002)	0.070(0.026)	0.028(0.004)	0.020(0.007)	0.003(0.001)	0.005(0.002)	0.007(0.002)	0.007(0.002)
Ce	0.044(0.012)	0.038(0.003)	0.030(0.002)	0.035(0.006)	0.109(0.016)	0.048(0.003)	0.032(0.005)	0.009(0.002)	0.013(0.005)	0.016(0.005)	0.012(0.0007)
Pr	0.062(0.018)	0.054(0.011)	0.049(0.005)	0.051(0.014)	0.116(0.015)	0.067(0.012)	0.049(0.005)	0.027(0.007)	0.035(0.014)	0.032(0.012)	0.019(0.001)
Nd	0.095(0.009)	0.085(0.012)	0.070(0.009)	0.082(0.008)	0.145(0.019)	0.083(0.004)	0.069(0.002)	0.049(0.006)	0.073(0.017)	0.074(0.012)	0.031(0.004)
Sm	0.158(0.019)	0.151(0.018)	0.096(0.037)	0.130(0.014)	0.182(0.013)	0.128(0.024)	0.072(0.007)	0.186(0.019)	0.235(0.036)	0.234(0.022)	0.120(0.018)
Eu	0.151(0.023)	0.138(0.006)	0.108(0.037)	0.124(0.016)	0.199(0.028)	0.105(0.016)	–	0.224(0.030)	0.316(0.025)	0.258(0.064)	–
Gd	0.191(0.021)	0.204(0.014)	0.125(0.021)	0.133(0.034)	0.172(0.038)	0.104(0.015)	0.103(0.008)	0.360(0.048)	0.433(0.046)	0.375(0.062)	0.221(0.021)
Tb	0.244(0.042)	0.218(0.050)	0.217(0.031)	0.147(0.031)	0.201(0.047)	0.160(0.037)	0.135(0.066)	0.633(0.12)	0.979(0.061)	0.649(0.080)	0.467(0.10)
Dy	0.229(0.022)	0.283(0.025)	0.227(0.008)	0.213(0.042)	0.259(0.044)	0.174(0.013)	0.204(0.045)	1.162(0.18)	1.642(0.28)	0.933(0.083)	0.826(0.065)
Ho	0.256(0.046)	0.216(0.055)	0.200(0.058)	0.194(0.028)	0.262(0.060)	0.198(0.046)	0.152(0.034)	1.602(0.28)	1.882(0.42)	1.241(0.26)	0.823(0.055)
Er	0.261(0.034)	0.198(0.020)	0.205(0.044)	0.217(0.048)	0.252(0.033)	0.226(0.037)	0.164(0.057)	1.992(0.13)	2.084(0.25)	1.272(0.14)	1.022(0.20)
Yb	0.345(0.162)	0.224(0.074)	0.251(0.032)	0.249(0.051)	0.331(0.098)	0.390(0.029)	0.244(0.020)	3.921(0.588)	3.144(0.51)	1.702(0.36)	1.653(0.24)
Lu	0.348(0.23)	0.292(0.049)	0.253(0.049)	0.237(0.045)	0.382(0.13)	0.112(0.067)	0.182(0.080)	3.945(0.99)	3.160(1.10)	2.338(0.66)	1.499(0.32)

All values and uncertainties calculated using data in Table 4

Table 6 Best fits for r_o, D_o and E obtained by regression of REE partition coefficients to the lattice strain model

P (GPa)	T (°C)	$^{(IV)}$Al	Ca	CaTs[a]	Wo[a]	r_o (Å)	D_o	E (GPa)
Clinopyroxene								
3	1,425	0.103	0.407	0.071	0.205	0.979 ± 0.005	0.32 ± 0.010	286 ± 40
3	1,475	0.088	0.354	0.068	0.181	0.979 ± 0.005	0.30 ± 0.010	281 ± 23
3	1,500	0.085	0.341	0.069	0.175	0.978 ± 0.005	0.24 ± 0.008	322 ± 32
3	1,525	0.082	0.334	0.065	0.172	0.978 ± 0.003	0.24 ± 0.005	240 ± 17
5	1,500	0.021	0.412	0.052	0.216	0.980 ± 0.003	0.27 ± 0.005	138 ± 7
5	1,600	0.043	0.386	0.062	0.201	0.980 ± 0.004	0.22 ± 0.007	224 ± 21
7	1,750	0.004	0.432	0.064	0.234	0.981 ± 0.004	0.17 ± 0.006	284 ± 32
				Py:Gss				
Garnet								
3	1,425			84:16		0.935 ± 0.003	4.72 ± 0.25	500 ± 43
3	1,475			86:14		0.930 ± 0.002	4.40 ± 0.18	461 ± 26
5	1,500			86:14		0.930 ± 0.003	2.70 ± 0.22	436 ± 52
7	1,750			86:14		0.930 ± 0.002	2.09 ± 0.14	522 ± 53

[a] CaTs and Wo components calculated using the method of Gaetani and Grove (1995)

Dunn 1993; Hauri et al. 1994; Johnson 1998; Klemme et al. 2002; Pertermann et al. 2004). $D^{cpx/liq}$ values for 3 GPa 97SB68 experimental clinopyroxenes are similar or slightly higher in magnitude and display comparable ratios to those in clinopyroxenes generated in peridotite experiments at 2.8 GPa (Salters and Longhi 1999). Figure 8 also shows the effect of temperature and pressure on 97SB68 $D^{cpx/liq}$ values. In general, $D^{cpx/liq}$ values increase with increasing pressure: the 5 GPa values at 1,500°C are higher than those at 3 GPa and similar temperatures. However, temperature appears to have a greater effect on $D^{cpx/liq}$ values: both the 3 and 5 GPa runs show decreasing $D^{cpx/liq}$ values with increasing temperature.

Figure 9 shows the effect of clinopyroxene major-element composition on a range of trace-element D values for the 3–7 GPa experimental runs. Only major elements that were found to have an effect on D values are shown; these are principally Ca and $^{(IV)}$Al (Fig. 9). The Ca contents (i.e. principally Wo components) of 97SB68 clinopyroxenes decrease with increasing temperature but remain relatively constant with increasing pressure (Fig. 2). At 3 and 5 GPa $D_{REE}^{cpx/liq}$ values for 97SB68 generally increase with Ca content (Fig. 9).

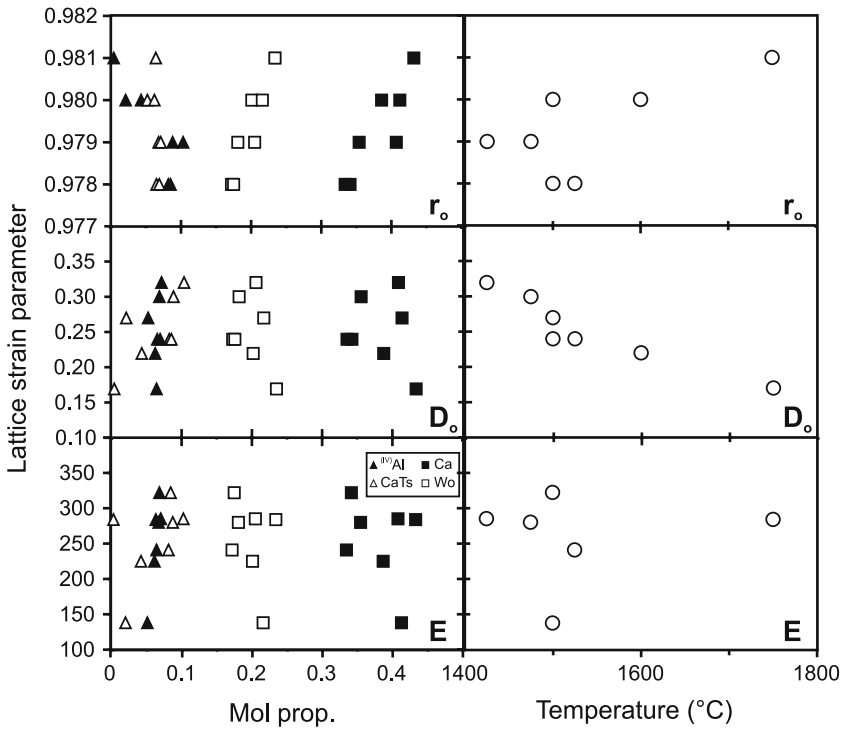

Fig. 5 Variation in $^{(IV)}$Al, Ca, CaTs and Wo contents and run temperatures of 97SB68 clinopyroxenes with lattice strain parameters r_o, D_o and E. Data are from Table 6

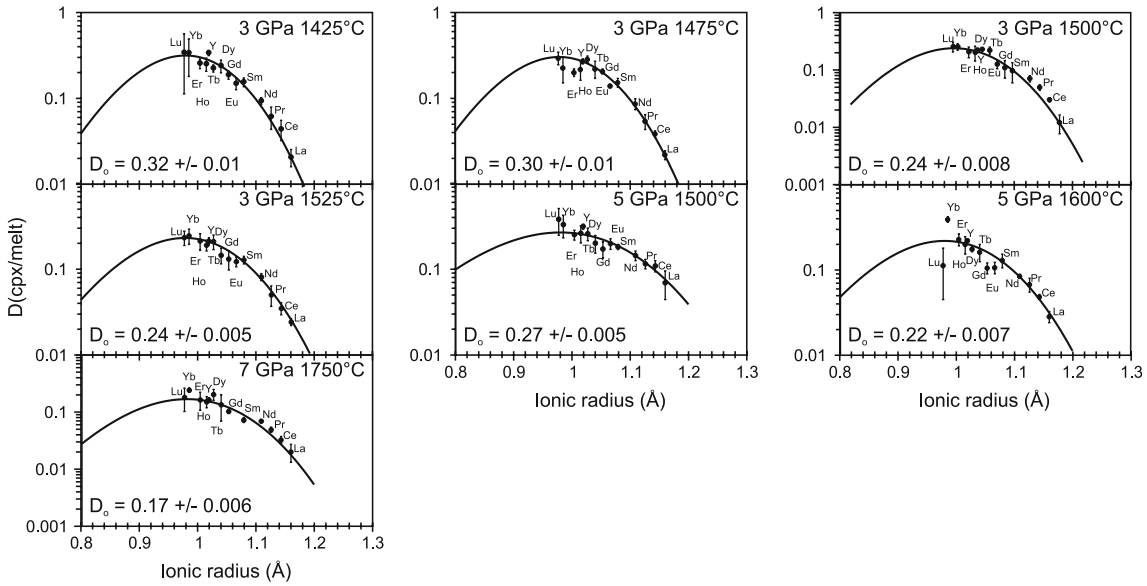

Fig. 6 Onuma diagrams (Onuma et al. 1968), showing 97SB68 partition coefficients (D) verses ionic radius (from Shannon 1976) of 3^+ ions entering the clinopyroxene M2 site. *Error bars* are 1 standard deviation and are shown where larger than the symbols. Data are from Tables 5 and 6

$D_{LREE}^{cpx/liq}$ values of 97SB68 clinopyroxenes exhibit a stronger correlation with increasing Ca content than they do with increasing $^{(IV)}$Al content (Fig. 9), in agreement with the results from the lattice-strain modelling (see above). $D_{Nb}^{cpx/liq}$ and $D_{Ti}^{cpx/liq}$ show little or no correlation with Ca. 97SB68 clinopyroxene Ca contents at 3 GPa generally fall between those of eclogites and peridotites at similar pressures and D values correlate with these variations over the compositions examined (Fig. 9).

Clinopyroxenes from 97SB68 experimental run products at 3–7 GPa (~$Ca_{0.2}Mg_{0.6}Fe_{0.2}Si_2O_6$) contain lower CaTs components than those from experiments on pyroxenites, eclogites and basalts, but are broadly comparable to those from peridotites (Fig. 10). The sub-calcic augites present in the experimental run products of 97SB68 have little Al in the fourfold co-ordination site (<0.1 mol prop.). In the 3 GPa runs, the clinopyroxenes exhibit a decrease in $^{(IV)}$Al with increasing temperature, but at 5 GPa $^{(IV)}$Al increases

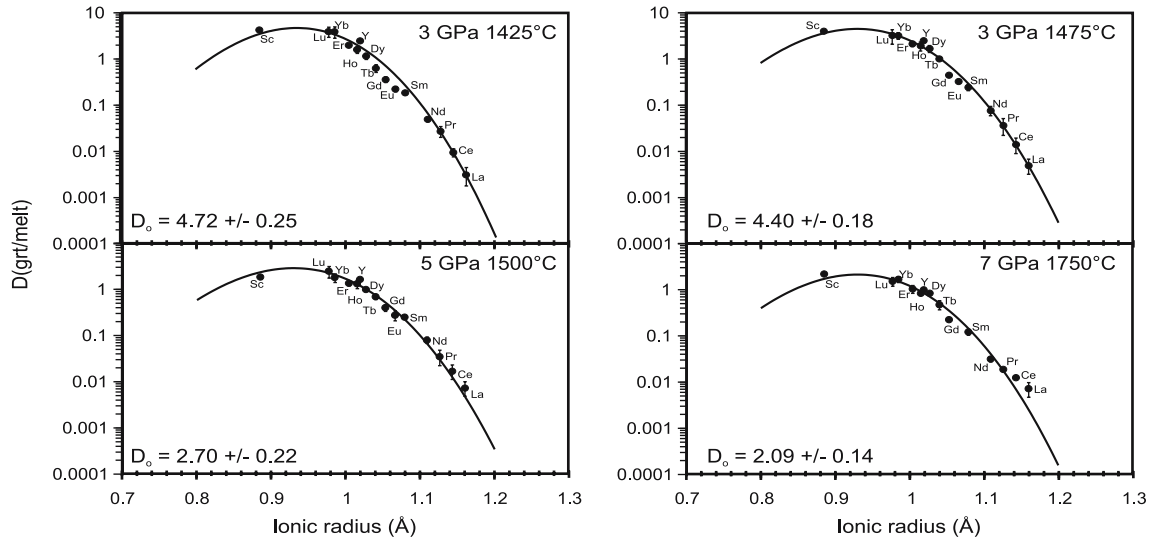

Fig. 7 Onuma diagrams (Onuma et al. 1968), showing 97SB68 partition coefficients (D) verses ionic radius (from Shannon 1976) of 3^+ ions entering the garnet X site. *Error bars* are 1 standard deviation and are shown where larger than the symbols. Data are from Tables 5 and 6

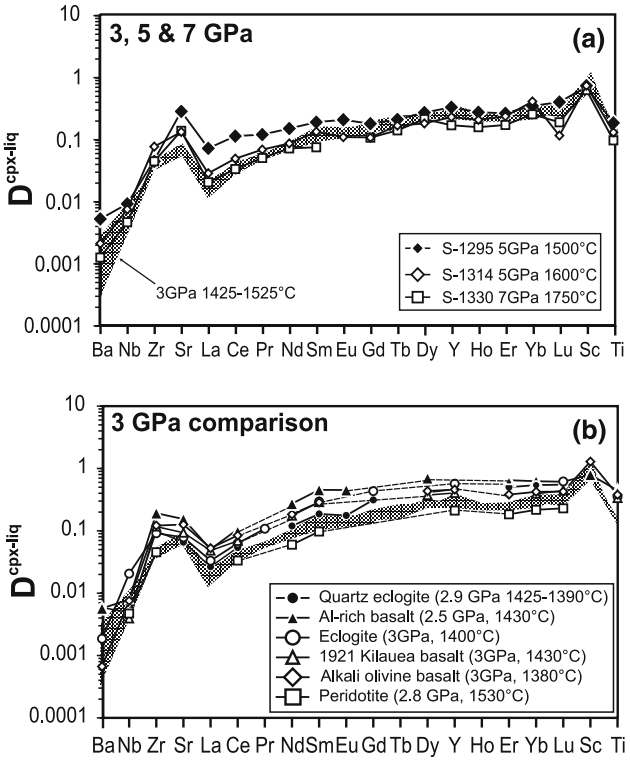

Fig. 8 **a** Comparison of incompatible trace-element $D^{cpx/liq}$ values of 97SB68 at 3 (*shaded field*), 5 and 7 GPa. Data are from Table 4. **b** Comparison of 97SB68 $D^{cpx/liq}$ values at 3 GPa (*shaded field*) with those from eclogite (Pertermann et al. 2004), basalt (Hart and Dunn 1993; Hauri et al. 1994; Johnson 1998) and peridotite (Salters and Longhi 1999) at similar pressures

with increasing temperature (Fig. 2). *D* values for HREEs, Y and Ti at 3 GPa follow the overall slightly positive correlations shown by peridotites and eclogites (Fig. 9). The weaker correlations shown in Fig. 9 suggest that Ca (i.e. Wo) is the dominant control on clinopyroxene *D* values because $^{(IV)}$Al (i.e. CaTs) contents are so low. In addition, Na was found to have little effect on *D* values of 97SB68 clinopyroxenes even though 97SB68 jadeite components are elevated compared to clinopyroxenes from peridotite experiments (Fig. 10). Both the lattice strain model and major-element correlations of 97SB68 clinopyroxenes suggest, while $^{(IV)}$Al and CaTs contents exert some influence, Ca in Wo is the principal control on clinopyroxene *D* values.

Major-element controls on garnet D values

In an idealised garnet solid-solution, $X_3Y_2Z_3O_{12}$, the X site hosts the divalent cations Fe^{2+}, Mg^{2+}, Ca^{2+} and Mn^{2+}, the Y site is occupied principally by Al^{3+}, Fe^{3+}, Cr^{3+} and Ti^{4+} and the Z site consists of Si^{4+}. Partitioning of the LREEs, Sr, Nb, Ta, U and Th into the garnet X site may be affected by the Ca and Mg contents of the garnet (van Westrenen et al. 1999, 2001; Klemme et al. 2002). Other trace-elements, such as Ti, Hf and Zr, are believed to enter the Y site by replacing Al.

In general, $D^{grt/liq}$ values correlate positively with Ca, Al and Fe^{2+} and negatively with Mg (Fig. 11), i.e. they exhibit a positive correlation with temperature (Fig. 3). $D^{grt/liq}_{LREE}$ values do not correlate with any of the major-elements and are not included in Fig. 11. $D^{grt/liq}_{Nb}$ values exhibit a scattered correlation with Ti, Mg and Ca and the control on Nb partitioning in the experimental run products of 97SB68 is unclear (only Ti is shown in Fig. 11). According to Pertermann et al. (2004), highly charged trace-element cations (e.g. Nb, Ta, Th, U) substitute into the garnet X site and have lower garnet-liquid ($D^{grt/liq}$) values for Ti-rich garnets (~1.5 wt.%) than Ti-poor garnets (≥ ~0.5 wt%). 97SB68 garnets at 3–7 GPa have TiO_2 contents between 0.7 and 1.2 wt.% (Fig. 3; Tuff et al. 2005) and fall within the range of low-Ti and high-Ti garnets defined by Pertermann et al. (2004). Peridotite garnet Ti contents are generally <0.1 wt.% (e.g. Takahashi et al. 1993; Salters and Longhi 1999). Although somewhat scattered, 97SB68 $D^{grt/liq}_{Nb}$ values fall within the range of those in garnets from peridotite and eclogite (Fig. 11).

In the 3–7 GPa ferropicrite run products, garnet is essentially a pyrope ($Mg_3Al_2Si_3O_{12}$) – almandine ($Fe_3Al_2Si_3O_{12}$) – grossular ($Ca_3Al_2Si_3O_{12}$) solid solution (Fig. 12). Garnets in natural peridotites have similar grossular and almandine, but higher pyrope contents ($Py_{70–88}Al_{17–20}Gr_{8–14}$) than garnets in ferropicrite run products. Eclogite garnets have higher grossular and lower almandine and pyrope contents ($Py_{20–70}Al_{10–50}Gr_{10–55}$; Fig. 12). The calculated $D^{grt/liq}$ values for the 3 GPa 1,425°C ferropicrite run products agree well with data reported for garnets from experimental charges of peridotites, eclogites and an olivine tholeiite at similar pressures and temperatures (Fig. 13; Salters and Longhi 1999; Klemme et al. 2002; Pertermann et al. 2004; Tuff et al. 2005). It is noted that at higher temperatures (1,475°C) 3 GPa $D^{grt/liq}_{LREE}$ values are higher (e.g. $D^{grt/liq}_{Ce}$ = 0.047) than those at lower temperatures (1,425°C) and approach the values obtained for an Al-rich basalt ($D^{grt/liq}_{Ce}$ = 0.065 at 1,430°C; Hauri et al. 1994). 97SB68 $D^{grt/liq}$ values follow the trends described above for clinopyroxenes in that they decrease with increasing temperature; this temperature effect appears to dominate the effect of pressure. In general, $D^{grt/liq}$ values for 97SB68 are more similar to those of per-

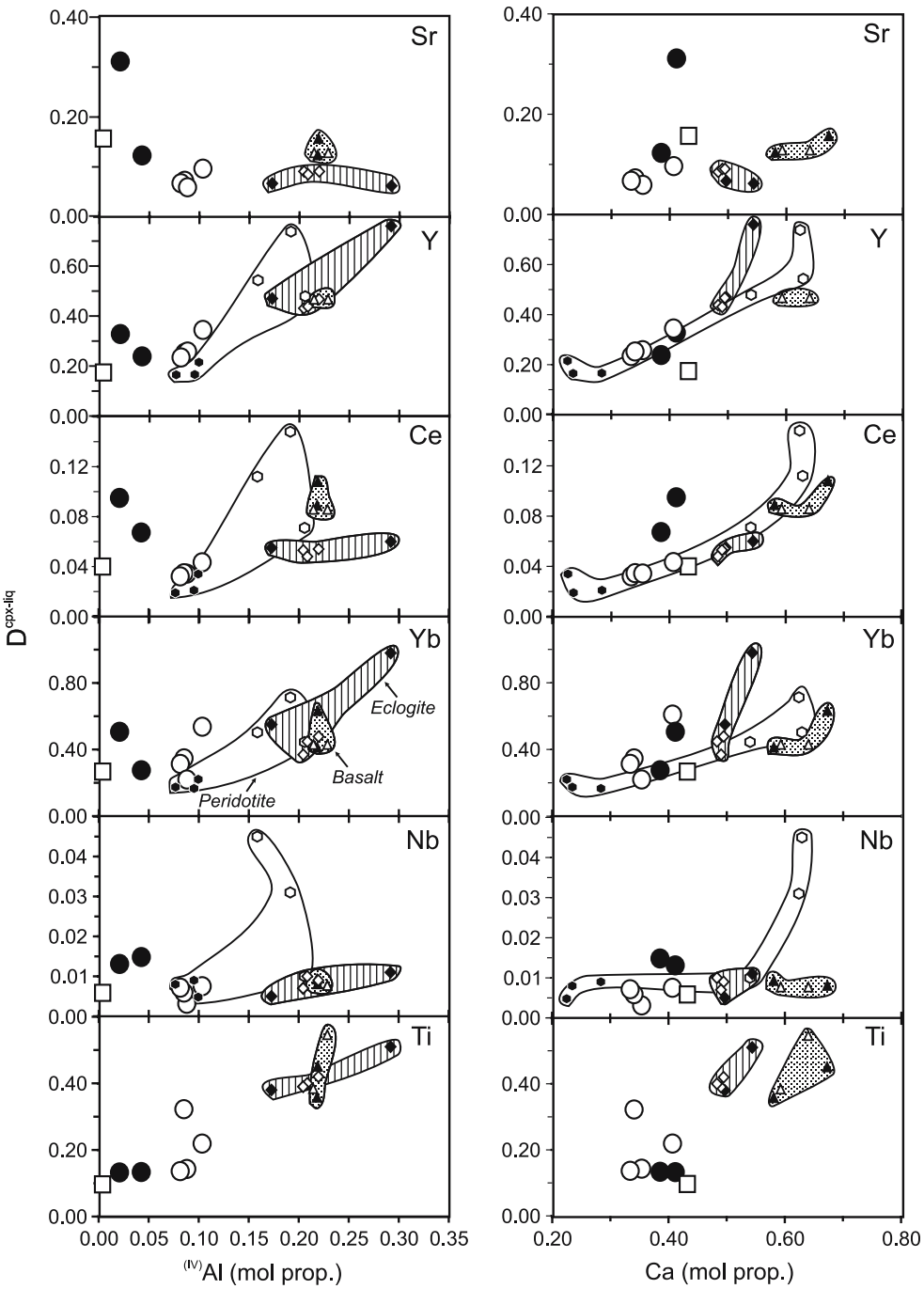

Fig. 9 Variation in $D^{\text{cpx-liq}}$ with major elements for 97SB68 clinopyroxenes from 3 to 7 GPa runs. Also shown are $D^{\text{cpx-liq}}$ values for clinopyroxenes in experiments on peridotite, eclogite and basalt. Also shown are data for: peridotite clinopyroxenes at <2 (*open hexagons*) and 2.8 GPa (*closed hexagons*, Salters and Longhi 1999); quartz eclogite clinopyroxenes at 3 GPa (*open diamonds*, Pertermann and Hirschmann 2002; *closed diamonds*, Pertermann et al. 2004); pyroxenes in alkali basalt at 1.7–2.5 GPa (*open triangles*, Hart and Dunn 1993) and in high-Al basalt at 3 GPa (*closed triangles*, Hauri et al. 1994)

idotites than eclogites. At 3 GPa 97SB68 experimental garnets have lower Ca and Al and higher Mg contents than eclogite garnets and exhibit lower HREE D values. This relationship between $D^{\text{grt/liq}}$ values and pyrope:grossular ratio is in agreement with the results of synthetic experiments (van Westrenen et al. 1999, 2001; Klemme et al. 2002) and suggests that the grossular content of 97SB68 garnets exerts a strong control on D values.

The effect of liquid composition on D values

The composition of a liquid that co-exists with solid phases (such as garnet and clinopyroxene) may also have an influence on trace-element partitioning (e.g. Hirschmann and Ghiorso 1994). Increased liquid Si contents are expected to increase trace-element partition coefficients. This is because increased Si causes a higher degree of polymerisation within the melt that

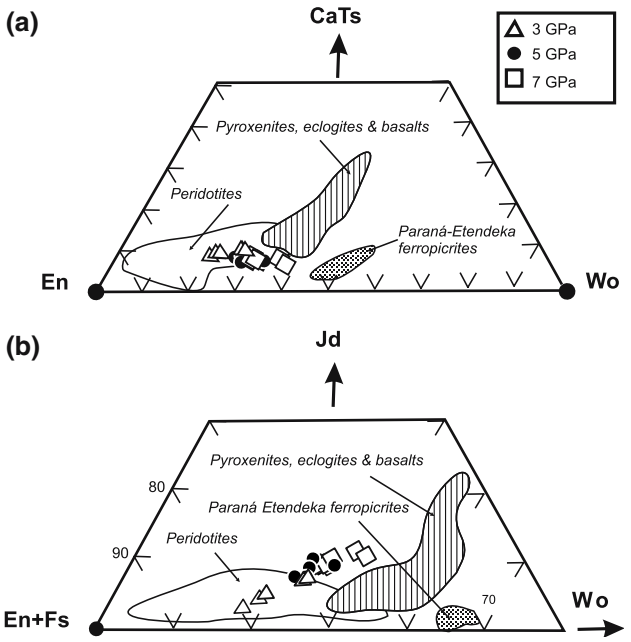

Fig. 10 Ternary diagram showing the compositions of 3–7 GPa 97SB68 clinopyroxenes in terms of **a** Wollastonite-Enstatite-Ca Tschermak and **b** Enstatite + Ferrosilite–Wollastonite–Jadeite components. Also shown are clinopyroxenes from Paraná-Etendeka ferropicrites (Gibson et al. 2000); experiments on basalts at 1.7–3 GPa (Hart and Dunn 1993; Hauri et al. 1994; Johnson 1998); quartz eclogites at 2–3 GPa (Pertermann and Hirschmann 2002, 2003a, b); silica undersaturated garnet pyroxenite at 2–5 GPa (Hirschmann et al. 2003; Kogiso et al. 2003) and peridotites at 2.8–7 GPa (Takahashi 1986; Walter 1998; Salters and Longhi 1999)

'forces' greater amounts of incompatible trace-elements into the co-existing crystals (Blundy and Wood 2003). It follows that increased liquid contents of silicate 'framework' elements (such as Si and Al) should cause an increase in $D^{\text{cpx-liq}}$ and $D^{\text{grt-liq}}$. In contrast, increasing the concentration of non-framework cations (such as Fe^{2+} and Mg) in the liquid may reduce the degree of polymerisation and allow higher contents of incompatible trace-elements. Although some correlation between clinopyroxene and garnet *D* values and framework elements was observed, the effect was minor compared to the effect of the major- element concentration on the minerals (Tuff 2005).

Bulk-partition coefficients

We have shown above that both garnet and clinopyroxene exert major controls on trace-element partitioning in 97SB68 run products. In order to examine the effect of these phases on trace-element ratios in mantle melts, we have calculated bulk-partition coefficients (bulk-*D*s).

97SB68 is believed to represent a primary mantle melt derived from a pyroxenite source (Tuff et al. 2005) and the liquidus phases should therefore be in equilibrium with the source lithology (Maaløe 2004). On the liquidus, the garnet:clinopyroxene ratio increases from 0:100 at 3 GPa to 25:75 at 5 GPa and 50:50 at 7 GPa (Table 7). Although calculated clino-

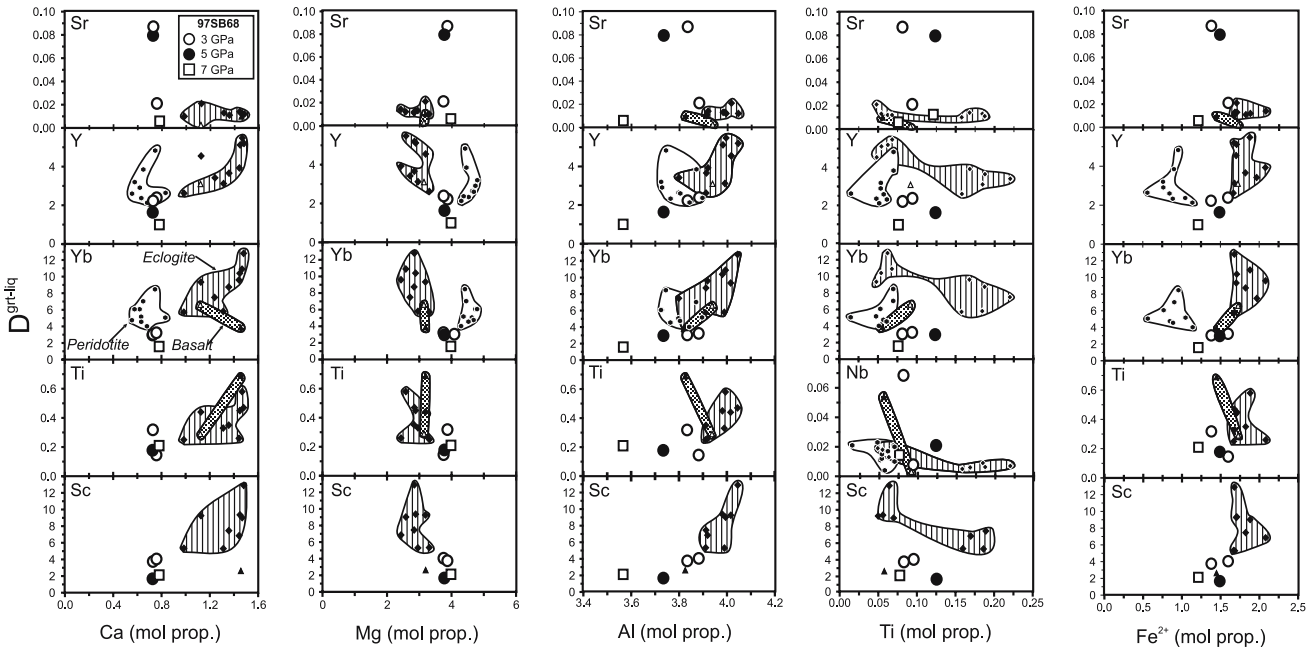

Fig. 11 Variation in $D^{\text{grt-liq}}$ with major-element contents of 97SB68 garnets from 3 to 7 GPa runs. Also shown are garnets from experimental runs on peridotite at 2.8 GPa (*closed hexagons*, Salters and Longhi 1999); quartz eclogite at 3 GPa (*closed diamonds*, Pertermann et al. 2004) and basalt at 2.5–3 GPa (*closed triangles*, Hauri et al. 1994; *open triangles*, Johnson 1998)

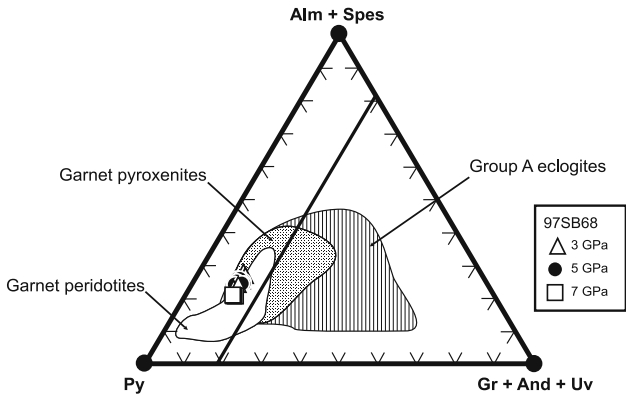

Fig. 12 Variation in garnet composition in terms of end-members: Pyrope (Py; $Mg_3Al_2Si_3O_{12}$); grossular (Gr; $Ca_3Al_2Si_3O_{12}$); andradite (And; $Ca_3Fe_2Si_3O_{12}$); uvarovite (Uv; $Ca_3Cr_2Si_3O_{12}$); almandine (Alm; $Fe_3Al_2Si_3O_{12}$) and spessartine (Spes; $Mn_3Al_2Si_3O_{12}$) after van Westrenen et al. (2001) and data sources therein. 97SB68 garnets at 3–7 GPa lie to the left of the 19% (Gr + And + Uv) line defined by van Westrenen et al. (2001). Data are from Tuff et al. (2005)

pyroxene and garnet modes near the 7 GPa liquidus are 4 % and 1%, respectively (Table 2), they are—within error (due to phase analysis and mass-balance calculations)—essentially present in equal amounts.

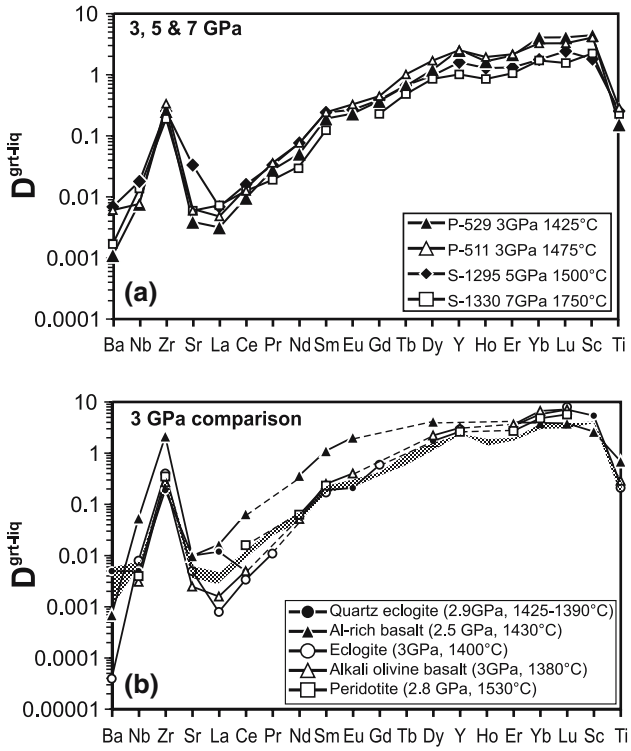

Fig. 13 **a** Comparison of incompatible trace-element $D^{grt/liq}$ values of 97SB68 at 3 (*shaded field*), 5 and 7 GPa. **b** Comparison of 97SB68 $D^{grt/liq}$ values at 3 GPa (*shaded field*) with those from eclogite (Pertermann et al. 2004), basalt (Hart and Dunn 1993; Hauri et al. 1994) and peridotite (Salters and Longhi 1999) at similar pressures

Bulk-partition coefficients for the ferropicrite run products were calculated using the liquidus modes in Table 7 and $D^{cpx/liq}$ and $D^{grt/liq}$ values that are as near to the liquidus at each pressure as possible (Table 5). At 5 GPa, however, we were only able to use 1,500°C trace-element partition coefficients because $D^{grt-liq}$ values for 5 GPa at liquidus temperatures were not determined (Table 5). Based on the trends in D values seen above (Figs. 8, 13), the lower temperature D values used at 5 GPa will be over-estimates of the true values, since 97SB68 D values are lowered with increasing temperature. Variations in bulk-D values reflect the changing relative abundances of garnet and clinopyroxene on the ferropicrite liquidus: the increase in modal garnet with pressure causes an increase in the bulk-Ds for the HREEs and Sc, so that the 7 GPa values are the highest. In contrast, bulk-D values are lowest for the LREEs at 7 GPa (Fig. 14). Bulk-D values for some LREE at 5 GPa are higher than those at 3 GPa. This may reflect the lack of $D^{grt-liq}$ values at liquidus temperatures.

At 3 GPa, bulk-partition coefficients in the 97SB68 run products are intermediate between those previously estimated for quartz eclogite and peridotite (Fig. 14; McKenzie and O'Nions 1991; Salters and Longhi, 1999; Pertermann et al. 2004). Peridotite is dominated by olivine (>50%), which has extremely low D values for the REEs; at high pressures (>3 GPa), modal proportions of garnet (<17%) and clinopyroxene (<36%) remain relatively low (e.g., Walter 1998) and incompatible trace-element bulk-D values are not expected to vary significantly with increasing pressure. Eclogites/pyroxenites become richer in garnet with increasing pressure (Hirschmann et al. 2003; Kogiso et al. 2003) and may exhibit similar trends in bulk-D values to 97SB68 at higher pressures, although this is not certain due to the lack of pyroxenite trace-element data at >3 GPa. In the absence of such data, trace-element partition coefficients for 97SB68 may be used to place important constraints on pyroxenite melting models.

Conclusions

We have shown that (1) trace-element partition coefficients for clinopyroxene and melt in garnet pyroxenites, generated in experiments on a high-Fe picrite, are lower than those in eclogites but higher than for peridotites at ~3 GPa; (2) trace-element partition coefficients for garnet and melt are higher for the LREE but lower for the HREE than those calculated

Table 7 Calculated bulk-partition coefficients for ferropicrite 97SB68, eclogite and peridotite

Run	3 GPa		5 GPa	7 GPa	Eclogite 3 GPa[b]	Garnet peridotite[c]	Peridotite 3 GPa[d]
Mode[a]	ol	0.00	0.00	0.00	0.00	0.60	0.60
	opx	0.00	0.00	0.00	0.00	0.20	0.17
	cpx	1.00	0.75	0.50	0.75	0.08	0.13
	grt	0.00	0.25	0.50	0.25	0.12	0.10
Sc		0.614	0.935	1.376	3.260	–	–
Ti		0.144	0.195	0.157	–	0.028	–
Sr		0.060	0.211	0.069	0.054	0.007	–
Y		0.216	0.622	0.571	1.380	–	0.340
Zr		0.035	0.095	0.114	0.223	–	0.064
Nb		0.009	0.011	0.009	0.007	0.001	0.003
Ba		0.003	0.006	0.002	0.006	–	–
La		0.024	0.054	0.014	0.021	0.006	–
Ce		0.035	0.086	0.022	0.044	0.011	0.005
Pr		0.051	0.095	0.034	–	0.019	–
Nd		0.082	0.127	0.050	0.164	0.033	0.016
Sm		0.130	0.195	0.096	0.233	0.048	0.045
Eu		0.124	0.214	–	0.242	0.064	–
Gd		0.133	0.223	0.162	0.501	0.084	–
Tb		0.147	0.313	0.301	–	0.115	–
Dy		0.214	0.428	0.515	1.029	0.153	–
Ho		0.194	0.507	0.487	–	0.206	–
Er		0.217	0.508	0.593	1.797	0.260	0.375
Yb		0.249	0.674	0.948	2.555	0.496	0.612
Lu		0.237	0.871	0.840	2.905	0.667	0.785

[a] Modes expressed as weight fraction on the liquidus (97SB68) and solidus (eclogite and peridotite). 97SB68 modes have been re-calculated from those in Table 2

[b] Preferred average eclogite of Pertermann et al. (2004)

[c] Garnet peridotite of McKenzie and O'Nions (1991)

[d] Peridotite of Salters and Longhi (1999) calculated by Pertermann et al. (2004)

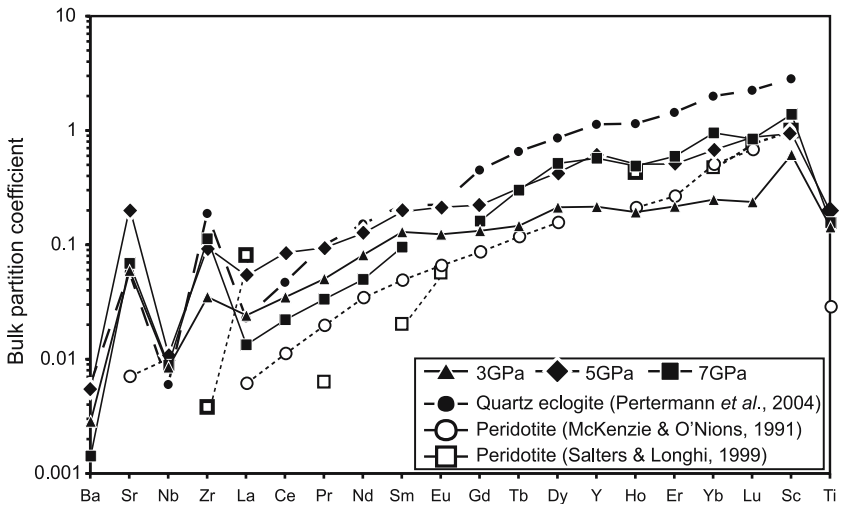

Fig. 14 Bulk-partition coefficients (D) of ferropicrite runs at 3, 5 and 7 GPa. Data are from Table 7. Also shown are bulk-Ds of a quartz eclogite at 2.9 GPa (Pertermann et al. 2004) and peridotite (McKenzie and O'Nions 1991; Salters and Longhi 1999)

from peridotite and eclogite experiments at ~3 GPa; (3) trace-element partition coefficients between garnet, clinopyroxene and melts decrease with increasing temperature.

The lattice strain modelling of 97SB68 clinopyroxenes suggests, while $^{(IV)}$Al and CaTs contents exert some influence, Ca in Wo is the principal control on clinopyroxene D values. Garnet D values are principally controlled by the grossular content. In contrast, the liquid major-element composition, for a given 97SB68 experimental run charge, has a minor effect on trace-element partitioning compared to the compositions of mineral phases.

Bulk-D values reflect the importance of modal mineralogy on trace-element partitioning. 97SB68 bulk-D values are intermediate between those for eclogites (garnet- and pyroxene-dominated mineralogy) and peridotites (olivine-dominated mineralogy) at 3 GPa. At 5 GPa, garnet is likely to become more prominent in pyroxenite mantle lithologies and will strongly affect partitioning, particularly of the HREEs and Sc. The trace-element partition coefficients that we

have determined for 97SB68 demonstrate this effect and may provide useful constraints in future numerical models of pyroxenite source regions.

Acknowledgments We thank R.N. Thompson for allowing us to use the ferropicrite sample 97SB68 in our investigation and E. Takahashi for the original experimental work. We are also grateful for the technical assistance and advice on SIMS and SEM analyses from J. Craven, S. Kasemann, R. Hinton and N. Cayzer. J. Taylor, Corpus Christi College and the University of Cambridge provided financial support for J.T. during this research project. We are grateful to J. Blundy and M. Bickle for their perceptive comments on an earlier version of the manuscript. This is Department of Earth Sciences contribution ES 8610.

References

Beattie P (1994) Systematics and energetics of trace-element partitioning between olivine and silicate melts: Implications for the nature of mineral melt partitioning. Chem Geol 117:57–71

Bennett SL, Blundy J, Elliott T (2004) The effect of sodium and titanium on crystal-melt partitioning of trace elements. Geochim Cosmochim Acta 68:2335–2347

Blundy JD, Wood BJ (1994) Prediction of crystal-melt partition coefficients from elastic moduli. Nature 372:452–454

Blundy J, Wood B (2003) Partitioning of trace elements between crystals and melts. Earth Planet Sci Lett 210:383–397

Blundy JD, Wood BJ, Davies A (1996) Thermodynamics of rare earth element partitioning between clinopyroxene and melt in the system CaO–MgO–Al_2O_3–SiO_2. Geochim Cosmochim Acta 60:359–364

Campbell IH (1998) The mantle's chemical structure: insights from the melting products of mantle plumes. In: Jackson I (ed) The Earth's mantle: composition, structure and evolution. Cambridge University Press, London, pp 259–310

Cordery MJ, Davies GF, Campbell IH (1997) Genesis of flood basalts from eclogite-bearing mantle plumes. J Geophys Res 102:20179–20197

Gaetani GA, Grove TL (1995) Partitioning of rare earth elements between clinopyroxene and silicate melt: crystal-chemical controls. Geochim Cosmochim Acta 59:1951–1962

Gallahan WE, Nielsen RL (1992) The partitioning of Sc, Y, and the rare-Earth elements between high-Ca pyroxene and natural mafic to intermediate lavas at 1-atmosphere. Geochim Cosmochim Acta 56:2387–2404

Garrido CJ, Bodinier J-L, Alard O (2000) Incompatible trace element partitioning and residence in anhydrous spinel peridotites and websterites from the Ronda orogenic peridotite. Earth Planet Sci Lett 181: 341–358

Gibson SA (2002) Major element heterogeneity in Archean to Recent mantle plume starting-heads. Earth Planet Sci Lett 195:59–74

Gibson SA, Thompson RN, Dickin AP (2000) Ferropicrites: geochemical evidence for Fe-rich streaks in upwelling mantle plumes. Earth Planet Sci Lett 174:355–374

Hart SR, Dunn T (1993) Experimental cpx/melt partitioning of 24 trace elements. Contrib Mineral Petrol 113:1–8

Hauri EH, Wagner TP, Grove TL (1994) Experimental and natural partitioning of Th, U, Pb and other trace elements between garnet, clinopyroxene and basaltic melts. Chem Geol 117:149–166

Herzberg C, O'Hara MJ (2002) Plume-associated ultramafic magmas of Phanerozoic age. J Petrol 43:1957–1883

Herzberg C, Zhang J (1996) Melting experiments on anhydrous peridotite KLB-1: compositions of magmas in the upper mantle and transition zone. J Geophys Res 101:8271–8295

Hill E, Wood BJ, Blundy JD (2000) The effect of Ca-Tschermaks component on trace element partitioning between clinopyroxene and silicate melt. Lithos 53:203–215

Hirose K, Kushiro I (1993) Partial melting of dry peridotites at high pressures: Determination of compositions of melts segregated from peridotite using aggregates of diamond. Earth Planet Sci Lett 114:477–489

Hirschmann MM, Ghiorso MS (1994) Activities of nickel, cobalt, and manganese silicates in magmatic liquids and applications to olivine liquid and to silicate metal partitioning. Geochim Cosmochim Acta 58:4109–4126

Hirschmann MM, Stolper EM (1996) A possible role for garnet pyroxenite in the origin of the ''garnet signature'' in MORB. Contrib Mineral Petrol 124:185–208

Hirschmann MM, Kogiso T, Baker MB, Stolper EM (2003) Alkalic magmas generated by partial melting of garnet pyroxenite. Geology 31:481–484

Johnson KTM (1998) Experimental determination of partition coefficients for rare earth and high-field-strength elements between clinopyroxene, garnet, and basaltic melt at high pressures. Contrib Mineral Petrol 133:60–68

Jones JH, McKay GA (1992) REE partitioning between pyroxene/liquid and garnet/liquid: parameterization using D_{Ca}. Eos (Trans AGU) 73:607 (Abstract)

Klemme S, Blundy JD, Wood BJ (2002) Experimental constraints on major and trace element partitioning during partial melting of eclogite. Geochim Cosmochim Acta 66:3109–3123

Keshav S, Gudfinnsson GH, Sen G, Fei Y (2004) High-pressure melting experiments on garnet clinopyroxenite and the alkalic to tholeiitic transition in ocean-island basalts. Earth Planet Sci Lett 223:365–379

Kogiso T, Hirose K, Takahashi E (1998) Melting experiments on homogeneous mixtures of peridotite and basalt: application to the genesis of ocean island basalts. Earth Planet Sci Lett 162:45–61

Kogiso T, Hirschmann MM, Frost DJ (2003) High-pressure partial melting of garnet pyroxenite: possible mafic lithologies in the source of ocean island basalts. Earth Planet Sci Lett 216:603–617

Kornprobst J (1980) A subsolidus high-pressure/high-temperature experimental study on a garnet-websterite assemblage exsolved from a single clinopyroxene accumulate at Freychinede (an alpine-type peridotite body), northern French Pyrénées. Colloques Internationaux du CNRS 272:245–252

Leitch AM, Davies GF (2001) Mantle plumes and flood basalts: enhanced melting from plume ascent and an eclogite component. J Geophys Res 106:2047–2059

Lundstrom CC, Shaw HF, Ryerson FJ, Phinney DL, Gill JB, Williams Q (1994) Compositional controls on the partitioning of U, Th, Ba, Pb, Sr and Zr between clinopyroxene and haplobasaltic melts—implications for Uranium series disequilibria in basalts. Earth Planet Sci Lett 128:407–423

Maaløe S (2004) The PT-phase relations of an MgO-rich Hawaiian tholeiite: the compositions of primary Hawaiian tholeiites. Contrib Mineral Petrol 148:236–246

McKay G, Wagstaff J, Yang SR (1986) Clinopyroxene REE distribution coefficients for Shergottites—the REE content of the Shergotty melt. Geochim Cosmochim Acta 50:927–937

McKenzie D, O'Nions RK (1991) Partial melt distributions from inversion of rare earth element concentrations. J Petrol 32:1021–1091

O'Neill HStC, Eggins SM (2002) The effect of melt composition on trace element partitioning: an experimental investigation of the activity coefficients of FeO, NiO, CoO, MoO_2 and MoO_3 in silicate melts. Chem Geol 186:151–181

Onuma N, Higuchi H, Wakita H, Nagasawa H (1968) Trace element partitioning between two pyroxenes and the host lava. Earth Planet Sci Lett 5:47–51

Pertermann M, Hirschmann MM (2002) Trace-element partitioning between vacancy-rich eclogite and silicate melt. Am Mineral 87:1365–1376

Pertermann M, Hirschmann MM (2003a) Partial melting experiments on a MORB-like pyroxenite between 2 and 3 GPa: constraints on the presence of pyroxenite in basalt source regions from solidus location and melting rate. J Geophys Res 108:2125. DOI 10.1029/2000JB000118

Pertermann M, Hirschmann MM (2003b) Anhydrous partial melting experiments on MORB-like eclogite: phase relations, phase compositions and mineral-melt partitioning of major elements at 2–3 GPa. J Petrol 44:2173–2201

Pertermann M, Hirschmann MM, Hametner K, Günther D, Schmidt MW (2004) Experimental determination of trace element partitioning between garnet and silica-rich liquid during anhydrous partial melting of MORB-like eclogite. Geochem Geophys Geosys 5. DOI: 10.1029/2003GC000638

Salters VJM, Longhi J (1999) Trace element partitioning during the initial stages of melting beneath mid-ocean ridges. Earth Planet Sci Lett 166:15–30

Salters VJM, Longhi JE, Bizimis M. (2002) Near mantle solidus trace element partitioning at pressures up to 3.4 GPa. Geochem Geophys Geosys 3. DOI: 10.1029/2001GC000148

Shannon RD (1976) Revised effective ionic radii and systematic studies of interatomic distances in halides and chalcogenides. Acta Crystallographica A 32:751–767

Takahashi E (1986) Melting of a dry peridotite KLB-1 up to 14 GPa: implications on the origin of peridotitic upper mantle. J Geophys Res 91:9367–9382

Takahashi E, Kushiro I (1983) Melting of a dry peridotite at high pressures and basalt magma genesis. Am Mineral 68:859–879

Takahashi E, Scarfe CM (1985) Melting of peridotite to 14 GPa and the genesis of komatiite. Nature 315:566–568

Takahashi E, Shimazaki T, Tsuzaki Y, Yoshida H (1993) Melting study of a peridotite KLB-1 and the origin of basaltic magmas. Phil Trans R Soc Lond A 342:105–120

Takahashi E, Nakajima K, Wright TL (1998) Origin of the Columbia River basalts: melting model of a heterogeneous plume head. Earth Planet Sci Lett 162:63–80

Tuff J (2005) Compositional heterogeneity of the Earth's mantle: experimental evidence from ferropicrites. Unpublished PhD thesis

Tuff J, Takahashi E, Gibson SA (2005) Experimental constraints on the role of garnet pyroxenite in the genesis of high-Fe mantle plume derived melts. J Petrol 46:2023–2058. DOI: 10.1093/petrologyegi046

Ulmer P (1989) The dependence of the Fe^{2+}-Mg cation-partitioning between olivine and basaltic liquid on pressure, temperature and composition – an experimental study to 30 kbars. Contrib Mineral Petrol 101:261–273

van Westrenen W, Blundy J, Wood B (1999) Crystal-chemical controls on trace element partitioning between garnet and anhydrous silicate melt. Am Mineral 84:838–847

van Westrenen W, Blundy JD, Wood BJ (2001) High field strength element/rare earth element fractionation during partial melting in the presence of garnet: implications for identification of mantle heterogeneities. Geochem Geophys Geosys 2. DOI: 10.1029/2000GC000133

Walter MJ (1998) Melting of garnet peridotite and the origin of komatiite and depleted lithosphere. J Petrol 39:29–60

Wood BJ, Blundy JD (1997) A predictive model for rare earth element partitioning between clinopyroxene and anhydrous silicate melt. Contrib Mineral Petrol 129:166–181

White RS, McKenzie D (1995) Mantle plumes and flood basalts. J Geophys Res 100:17543–17585

Yaxley GM (2000) Experimental study of the phase and melting relations of homogeneous basalt + peridotite mixtures and implications for the petrogenesis of flood basalts. Contrib Mineral Petrol 139:326–338

Yaxley GM, Green DH (1998) Reactions between eclogite and peridotite: mantle refertilisation by subduction of oceanic crust. Schweiz Mineral Petrogr Mitt 78:243–255